ENGINEERING BIOMEDICAL TECHNOLOGIES FOR THE DEVELOPING WORLD

A Dissertation

Presented to the Faculty of the Graduate School

of Cornell University

In Partial Fulfillment of the Requirements for the Degree of

Doctor of Philosophy

by

Sasank Vemulapati

August 2019

ENGINEERING BIOMEDICAL TECHNOLOGIES FOR THE DEVELOPING WORLD

Sasank Vemulapati, Ph. D.

Cornell University 2019

The global healthcare landscape is experiencing a shift with an increasing demand for decentralized testing. Diagnostic testing is moving from the benchtop to the bedside and there is a need for translational medical tools to help usher in the generation of personalized medicine. Point-of-care medical devices have become a powerful tool to help address this growing need and can help deliver high-quality diagnostic testing at lower costs and greater convenience in comparison to conventional laboratory techniques. Point-of-care devices have also emerged as a suitable platform for use in resource limited settings where access to state-of-the-art medical equipment is scarce. In this dissertation, I detail the design and development of three unique biomedical technologies: Nutriphone, H.E.R.M.E.S and cAST. These technologies were created and developed with the specific intention of advancing diagnostic testing at the point-of-care with extended application for use in resource-limited environments. While there are similar themes in the design philosophy of the three technologies, they address entirely different areas of interest; Nutriphone enables rapid assessment of Vitamin D deficiencies, H.E.R.M.E.S enables quick and efficient pre-diagnostic sample preparation for blood-based testing and cAST offers accelerated assessment of antimicrobial resistance in bacterial organisms. I will highlight the underlying technical principles and the key innovations that we were able to demonstrate along with initial clinical results that make them promising platforms worthy of further development.

BIOGRAPHICAL SKETCH

Sasank Vemulapati was born in Orlando, FL. When he was 5, he moved from Orlando to India and grew up in the lively city of Hyderabad until he was 17. He then matriculated to the University of Illinois at Urbana-Champaign and received a Bachelor of Science in Mechanical Engineering in 2015. He went on to pursue his graduate studies at Cornell University in Mechanical Engineering with a focus on biomedical engineering. His time at Cornell was spent as a member of David Erickson's lab group and he worked on developing unique and interesting biomedical technologies aimed at use for the developing world. He received his Master of Science degree in 2017 and completed his doctorate degree in the summer of 2019. Upon completion of his degree, he will pursue a career in product design.

ACKNOWLEDGMENTS

There would be no beginning or end if it weren't for the love and support of my parents, Udaya and Jayanti Vemulapati. Eight years ago, they gave me the confidence I needed to leave home and live alone 9000 miles away. Their support has never wavered and for that, I will be eternally grateful. A special mention to Vibhakar Vemulapati for constantly reminding me to challenge my assumptions.

I would like to thank my advisor, David Erickson for his excellent mentorship and support throughout my time in his lab. David helped nurture an understanding for research in my early years and gave me the creative freedom I needed as I matured. I would also like to thank my committee members, Saurabh Mehta and Ankur Singh for their support and the high-level input they have given me over the years.

I would also like to thank Joseph Kalman, who helped me through my first research experience in 2013. Joseph showed me that to be successful in research, one needs a great work ethic and an even greater sense of humor.

I thank my lab mates in the Erickson Group for their support. In 2015, a brief phone call with Ryan Snodgrass helped me decide that Cornell was the right fit for me. Once I was here, Seoho Lee and Dakota O'Dell helped me feel included in the Erickson Research Group and gave me a good sense of what it meant to be successful in graduate school. A special mention to Elizabeth Rey and Rick Wang for being helpful collaborators on my research projects and making teamwork seem easy.

I'd like to thank the friends I've made in Ithaca, who made the cold winters seem less dreary. Tanner Pearson, who I lived with for three years and who shares a lot of my interests. Joseph Corbett-Davies, a fellow "international" student who travelled with me during thanksgiving breaks and Gabriel Soto who was always around in case I needed a musical escape. Finally, I'd like to thank Josephine Gonzales who helped bring a sense of balance and perspective to my daily life.

TABLE OF CONTENTS

LIST OF FIGURES

LIST OF TABLES

LIST OF ABBREVIATIONS

µg - Microgram

3D – Three Dimensional (Printing)

AST – Antibiotic Susceptibility Testing

ATCC – American Type Culture Collection

AuNP- Gold Nanoparticles

BSA – Bovine Serum Albumin

cAST – Capillary Antibiotic Susceptibility Testing

CFU – Colony forming Units

CLIA – Certificate for Laboratory Improvement Amendment

CLSI – Clinical and Laboratory Standards Institute

CMOS – Complementary Metal-Oxide-Semiconductor

CV – Coefficient of Variation

DMSO – Dimethyl Sulfoxide

FDA – Food and Drug Adminstration

Gen – Gentamicin

HD – High Definition

H.E.R.M.E.S – High Efficiency Rapid Magnetic Erythrocyte Separator

ID – Inner Diameter

Kan – Kanamycin

L – Length

LC/MS-MS- Tandem Liquid Chromatography and Mass Spectrometry

LED- Light Emitting Diode

mg - Milligram

MIC – Minimum Inhibitory Concentration

mL - Milliliter

OD – Outer Diameter/Optical Density

PBS – Phosphate Buffered Saline

PCR – Polymerase Chain Reaction

RIA – Radio Immuno Assay

ROC – Receiver Operator Characteristic

T/C – Test over Control Line

TBS – Tris Buffered Saline

CHAPTER ONE

INTRODUCTION

1.1 Overview

Personalized medicine is the future of healthcare. The demand for diagnostic testing is moving away from large established institutions like hospitals and closer to the home. To address this growing demand, diagnostic technologies must translate from the benchtop to the bedside and adapt to be suitable for use in low-complexity testing environments. Over the past two decades, this movement has been broadly classified as "Point-of-care" testing and has become the central idea around which medical technologies have started to evolve around. Point-of-care testing (POC) can help deliver high-quality diagnostic testing at lower costs and greater convenience in comparison to conventional laboratory method. Further, POC testing represents a suitable platform that can elevate testing standard standards in resource limited settings where access to state-of-the-art medical equipment is scarce.

In this dissertation, I detail the design and development of three unique biomedical technologies that are appropriate for use at the point-of-care: Nutriphone H.E.R.M.E.S and cAST. I dedicate each chapter of my thesis to one of each of the above-mentioned technologies. These technologies were designed with the specific intention of being limited-resource friendly and while there are similar themes in the design philosophy, each technology addresses an entirely different area of interest. I will first discuss the Nutriphone, which was designed for the rapid assessment of Vitamin D deficiencies in blood. Then I will detail my invention, H.E.R.M.E.S, which is a unique alternative to perform quick and efficient pre-diagnostic sample preparation for blood-based testing. Finally, I will detail cAST, a platform we developed that offers

accelerated assessment of antimicrobial resistance in bacterial organisms. In each case, we validated the technologies with relevant samples in order to further cement their applicability for use in translational medical environments.

1.2 A quantitative assay for the assessment of Vitamin D_3 deficiencies

Chapter 2 of this dissertation elaborates on the development and validation of a rapid diagnostic test for the assessment of Vitamin D deficiencies. Vitamin D is necessary for the healthy growth and development of bone and muscle. Vitamin D deficiency, which is present in 42% of the US population, is often undiagnosed as symptoms may not manifest for several years and long-term deficiency has been linked to osteoporosis, diabetes and cancer. Currently the majority of vitamin D testing is performed in large-scale commercial laboratories which have high operational costs and long times-to-result. Development of a low-cost point-of-need assay could be transformative to deficiency analysis in limited-resource settings. The best biomarker of vitamin D status, 25hydroxyvitamin D_3 ($25(OH)D_3$), however, is particularly challenging to measure in such a format due to complexities involved in sample preparation, including the need to separate the marker from its binding protein. In this chapter, we present a rapid diagnostic test for the accurate, quantitative assessment of $25(OH)D_3$ in finger-stick blood. The assay is accompanied by a smartphone-assisted portable imaging device that can autonomously perform the necessary image processing. To achieve accurate quantification of $25(OH)D_3$, we also demonstrate a novel elution buffer that separates $25(OH)D_3$ from its binding protein in situ, eliminating the need for sample preparation. We highlight the validation of the assay with human serum and blood samples. In human trials, the accuracy of our platform is 90.5%.

1.3 Development of a magnetic bead-based blood-plasma separation system

In Chapter 3, I detail the design and development of the High Efficiency Rapid Magnetic Erythrocyte Separator (H.E.R.M.E.S), a rapid low-cost technology that can perform the separation of red blood cells from plasma at a fraction of the time and cost of that of a centrifuge. H.E.R.M.E.S was designed to help blood-testing cope with the increasing demand for CLIA-waived testing facilities that offer diagnostic capabilities at lower costs and greater convenience than traditional laboratory testing. While several new diagnostic tools have emerged to fulfill testing requirements in these environments, centrifuges have been stymied from transitioning to the point-of-need as the US Food and Drug Administration (FDA) classifies them as mostly unsuitable for use in CLIA-waived environments. Limitations in sample processing capabilities adversely affects the ability for CLIA-waived testing environments to offer a broad testing portfolio and present-day diagnostics are bottlenecked by the requirement for centrifugation. H.E.R.M.E.S is a unique method to perform rapid, low-cost sample processing and can perform the separation of red blood cells from plasma at a fraction of the time and cost of that of a centrifuge. In Chapter 2, we demonstrate that H.E.R.M.E.S is able to obtain highly-pure plasma (greater than 99.9% purity) at less than 2 minutes per test. H.E.R.M.E.S was originally designed for use with rapid diagnostic tests such as lateral flow assays, however, through the development of the technology, we discovered that it is capable of being incorporated with any present-day diagnostic technology. We also prove that it is superior to existing alternatives to centrifugation by validation with a ferritin lateral flow test.

1.4 A novel approach for the detection of antimicrobial resistance in bacteria

In the final chapter, I discuss our initial efforts at developing a detection platform for the rapid assessment of antimicrobial resistance in infectious bacterial organisms. Antibiotic resistance is a major global health concern due to an overuse of antibiotics in medicine and in agriculture. It is estimated that by 2050, 10 million people will die from antibiotic resistant bacteria. For patients with septic shock, it is estimated that for every hour that effective antibiotic treatment is delayed, the survival rate drops by 7.6%. There is a need for effective diagnostic tools that can enable rapid and accurate assessment of antibiotic resistance in order to facilitate the immediate application of appropriate antibiotic therapy. This is of particular importance for resource-limited settings where access to state-of-the-art treatment and equipment is limited. We describe the design of cAST, a unique approach that offers accelerated assessment of antibiotic resistance. cAST uses a capillary form factor that enhances the growth rate of the bacterial cells, thereby expediting the time to readout. Further, cAST was built using a combination of off-the-shelf parts and custom 3D printed holders to enable low-cost, real-time assessment of bacterial viability with the help of a portable spectrometer. We first demonstrate that capillary incubation is superior to standard bacterial growth in a well and then detail the validation of our platform with 5 different clinically relevant infectious organisms. We demonstrate detection of bacterial growth within 4-8 hours and detail the future work that can be done in order to further improve the design of cAST. The underlying technology of cAST makes it immediately applicable to existing clinical methods used to determine AST and can be further simplified for qualitative use in resource-limited settings.

CHAPTER 2

A QUANTITATIVE POINT-OF-NEED ASSAY FOR THE ASSESSMENT OF VITAMIN D_3 DEFICIENCY[†]

2.1 Abstract

Vitamin D is necessary for the healthy growth and development of bone and muscle. Vitamin D deficiency, which is present in 42% of the US population, is often undiagnosed as symptoms may not manifest for several years and long-term deficiency has been linked to osteoporosis, diabetes and cancer. Currently the majority of vitamin D testing is performed in large-scale commercial laboratories which have high operational costs and long times-to-result. Development of a low-cost point-of-need assay could be transformative to deficiency analysis in limited-resource settings. The best biomarker of vitamin D status, 25hydroxyvitamin D_3 ($25(OH)D_3$), however, is particularly challenging to measure in such a format due to complexities involved in sample preparation, including the need to separate the marker from its binding protein. Here we present a rapid diagnostic test for the accurate, quantitative assessment of $25(OH)D_3$ in finger-stick blood. The assay is accompanied by a smartphone-assisted portable imaging device that can autonomously perform the necessary image processing. To achieve accurate quantification of $25(OH)D_3$, we also demonstrate a novel elution buffer that separates $25(OH)D_3$ from its binding protein in situ, eliminating the need for sample preparation. In human trials, the accuracy of our platform is 90.5%.

[†]Reprinted with permission from Vemulapati, S., Rey, E., O'Dell, D., Mehta, S., and Erickson, D. *Scientific Reports* 7 (2017).

2.2 Introduction

Vitamin D refers to a group of fat soluble secosteroids responsible for promoting absorption of calcium, phosphate and zinc in the body[1,2]. It is also essential for the healthy growth and maintenance of bone and muscle[3]. Vitamin D deficiency causes rickets in children[4] and low levels of vitamin D have been attributed to diabetes, heart disease, cancer and osteoporosis in adults[5]. Vitamin D is also critical for ensuring optimal immune function; for example, vitamin D is required for producing antimicrobial peptides such as cathelicidin, necessary to combat pathogens such as *Mycobacterium tuberculosis* in human macrophages[6]. Deficiency is defined by evaluating the serum concentrations of 25-hydroxyvitamin D, or 25(OH)D, a pro-hormone that is produced in the liver by hydroxylation of cholecalciferol, the biologically inert form of vitamin D that is produced in the skin. 25(OH)D is the major circulating form of vitamin D and is considered the best indicator of holistic vitamin D status. Supplemental vitamin D is available in two forms: ergocalciferol (vitamin D_2) and cholecalciferol (vitamin D_3). Even though commonly prescribed supplements contain either vitamin D_2 or vitamin D_3, it has been demonstrated that cholecalciferol has a higher efficacy at raising the total serum 25(OH)D status in individuals[7,8]. As a result, many of the supplements now on the market contain cholecalciferol. The Endocrine Society guidelines suggest that individuals with serum concentration of 25(OH)D greater than 75 nmol/L can be considered healthy while those with values between 50 and 75 nmol/L are insufficient and lower than 50 nmol/L are deficient[9].

In the United States, the prevalence of vitamin D deficiency rate is estimated at 42%, with a higher incidence amongst the African American (82%) and Hispanic (69%) population[10]. Deficiency can be corrected with supplementation and dietary changes particularly when detected early; however, many people are unaware of their status due to the lack of easy to access methods for quantifying 25(OH)D_3 levels in human serum.

Point-of-care vitamin D deficiency testing remains a significant challenge due to the presence of vitamin D binding protein, a carrier protein that helps transport 25(OH)D in blood. 95-99% of available 25(OH)D in blood is bound to vitamin D binding protein[11,12] and due to the nature of the strong hydrophobic bond between them, it is not possible to assess an individual's vitamin D status without separating the two from each other. Furthermore, vitamin D binding protein is always present in significant molar excess in blood and has no correlation with the amount of circulating 25(OH)D[13–15]. As a result, it cannot be used as a target itself, a scheme which has been adopted for targets such as vitamin A[16–19].

Current clinical methods for quantitation of 25(OH)D can be broadly divided into chromatographic methods with (LC/MS-MS: Liquid Chromatography Tandem Mass Spectrometry) and without (HPLC: High Performance Liquid Chromatography) mass spectrometric detection and competitive immunoassays such as RadioImmunoAssay (RIA). These techniques are expensive and time consuming due to the need for specialized equipment and personnel and the necessity to separate and remove vitamin D binding protein presents further complications by requiring elaborate sample preparation. Usually the sample is treated and incubated (for ~1 hour) with large amounts of organic solvents such as acetonitrile to perform the separation step. Further, organic solvents cannot be used directly with blood as they cause lysis of blood cells, and require that the blood be centrifuged into serum. Standard protocols also require an additional centrifugation step after the organic solvents are added in order to remove the precipitated protein. These tedious sample preparation requirements combined with the need for specialized equipment pose a severe limitation for the development of point-of-need tests for the assessment of vitamin D status.

In recent years, several research groups have employed microfluidic techniques to develop low cost methods to assess micronutrient status at the point-of-need. A

microfluidic chip that was able to perform the detection of ferritin and CRP in human serum samples was demonstrated by Kartalov *et al*[20]. Similarly, Dimov et al exhibited the "stand-alone self-powered integrated microfluidic blood analysis system (SIMBAS)" for detection of vitamin B_6[21]. While these works have demonstrated excellent proof of concepts for use at the point of care, they are limited by their inability to perform blood processing on chip and the need for expensive imaging equipment. Lee *et al.*[22] demonstrated the vitamin AuNP-based Immunoassay Device (vitaAID), a system for quantification of vitamin D levels using a smartphone. In that work, a novel gold nanoparticle-based immunoassay architecture was developed and analyzed by a smartphone camera, enabling quantification of serum samples without the need for expensive lab equipment. Even though the method helped transition vitamin D testing out of the lab, the technique was limited by its inability to perform blood processing on chip and non-trivial incubation time (~6 hours).

In this work, we present a rapid diagnostic test that is capable of accurate, quantitative assessment of vitamin D status. Our test focuses on quantification of 25(OH)D_3, the largest component of circulating 25(OH)D, in the deficient range (< 50nmol/L), as that is where the greatest need is. Quantitative ability is necessary in the deficient range to help distinguish between individuals who are severely and moderately deficient. In order to maintain compatibility with existing manufacturing techniques, we developed our diagnostic test as a lateral flow assay. Furthermore, our diagnostic test is integrated into a smartphone-assisted imaging platform which allows for easy operation and hassle-free access to test results. In addition to being capable of processing blood on strip, our test incorporates a novel elution buffer that is compatible with lateral flow assays to achieve separation of 25(OH)D_3 from its binding protein in situ, eliminating the need for any sample preparation. We show reliable quantification of physiologically

relevant vitamin D_3 levels in standard solutions, commercial calibrators, human serum and finger stick blood.

2.3 Results

2.3.1 Vitamin D3 diagnostic test protocol

The system consists of a vitamin D_3 diagnostic test, custom made cassette that houses the test and a portable reader (TIDBIT) (See Figure 1). The TIDBIT has been designed so that when the cassette is inserted into the device, it is aligned with a CMOS camera that automatically captures an image of the test area. The TIDBIT can be operated via a smartphone or computer application and can be controlled with the help of the Nutriphone application. Once the image is taken, a custom python script automatically crops the image and deduces the ratio of intensities of the test line to the control line, or T/C ratio (See Figure 2B and 2C). The T/C ratio is correlated to a value of 25(OH)D_3 by using a calibration curve, that is determined prior to testing by analyzing samples of known 25(OH)D_3 values.

To run a vitamin D_3 test, the user starts the Nutriphone application on the device of choice and follows the instructions. First the user applies a small amount (4µL) of elution buffer on the edge of the sample pad. The user then collects 40µL of blood from a finger prick and places it onto the sample collection pad. After allowing for the blood to separate into serum and mix with the elution buffer, the user is prompted by the smartphone application to apply 15µL of running buffer for the filtered serum to enter the conjugate pad. After another short period of incubation, the user is again prompted to add 25 µL of running buffer to start the test. Following this step, the user must place the cassette in the TIDBIT, which automatically images and analyzes the test strip when the test and control lines are fully developed. Briefly, a grayscale image is taken using the TIDBIT and processed by a python script to filter out the noise using a Gaussian

filter. The noisy 2D image is filtered and converted to the grayscale, followed by a median filtering process to convert the 2D image into a 1D array, reducing the task to analyzing a 1D digital signal. The test and control lines of concentrated AuNP – anti 25(OH)D_3 are detected as local minima on the intensity plot. The respective peak values can be used to calculate a T/C ratio.

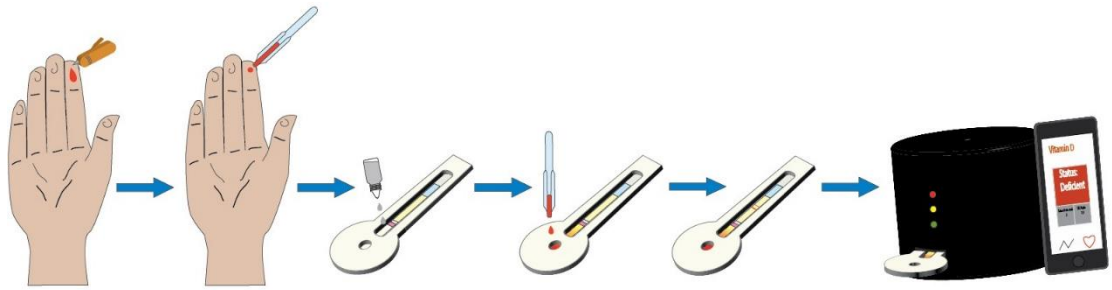

Figure 1: Protocol for Vitamin D_3 diagnostic test. The TIDBIT is depicted as the last image on the right.

2.3.2 Design and implementation of a protein elution buffer:

Vitamin D binding protein interferes with the capture and quantification of 25(OH)D_3 via traditional immunoassay techniques. Commercial tests such as the DiaSorin RIA call for mixing the sample with 10X the amount of acetonitrile, an organic solvent, in order to liberate all 25(OH)D_3 in the sample from the binding protein[23]. This method cannot be directly translated for application with a low-cost point-of-need lateral flow platform for several reasons. Firstly, organic solvents cause lysis of red blood cells[24], making it unsuitable for use with blood samples; the sample must be first spun down into serum via centrifugation, a process that is difficult to perform in point-of-need settings. Secondly, if not neutralized or removed prior to running the test, acetonitrile could negatively affect the conjugated gold nanoparticles and the dispensed reagents on the test and control lines as the antibodies present are prone to denaturation themselves.

Finally, adding large amounts of organic solvent is particularly unsuitable for lateral flow platforms, as they may adsorb to the nitrocellulose membrane and alter its wetting properties [26]. It was therefore necessary to develop an elution buffer that could denature binding protein in the sample without lysing blood cells while maintaining compatibility with the nitrocellulose membrane, the conjugated nanoparticles and the dispensed reagents.

In order to perform the separation of 25(OH)D_3 from its binding protein, our diagnostic test takes advantage of carefully optimized organic solvents and low pH buffers, which are known to be effective at denaturing proteins. After assessing a number of possible combinations, we decided on a combination of Dimethyl sulfoxide (DMSO), ethanol and a low pH acetate buffer. We hypothesize that DMSO and ethanol are able to unfold vitamin D binding protein while also serving as organic solvents to stabilize the liberated 25(OH)D_3[25]. This unfolding effect is further enhanced in the presence of a low pH buffer as most proteins undergo destabilization at low pH[26]. As seen in Figure 3B, there is no relationship between [25(OH)D_3] and the T/C ratio when samples are tested for vitamin D_3 without the use of any elution buffer.

2.3.3 Vitamin D3 diagnostic test architecture and principles:

The vitamin D_3 diagnostic test seen in Figure 2 consists of a: blood filtration membrane, a conjugate pad that dry stores gold nanoparticle conjugates (AuNP – anti 25(OH)D_3), a spacer pad that allows for incubation of the sample with the elution buffer and the conjugates, a nitrocellulose membrane that houses immobilized 25(OH)D_3-BSA and secondary antibodies and a cellulose fiber absorbent pad respectively. When applicable, the blood filtration membrane can be substituted for a cellulose fiber pad to perform testing in human serum. Our test strip adopts a competitive type architecture as

$25(OH)D_3$ is unable to bind to more than one antibody at a time due to its small size (~350 Daltons).

The architecture of the diagnostic test was designed in order to prevent any need for specialized sample preparation. Prior to starting the test, the user dispenses a small amount of elution buffer onto the front edge of the blood filtration membrane to prevent the interaction of the elution buffer and the red blood cells present in the blood sample. Once the user dispenses the blood on the sample pad, it automatically flows forward through the filtration paper and separates into serum while simultaneously mixing with the elution buffer. This causes bound $25(OH)D_3$ to be released from the binding protein present in the sample. After the first instance of running buffer is applied, the sample enters the conjugated pad and the unbound $25(OH)D_3$ interacts with the AuNP-anti $25(OH)D_3$ conjugates. This step is critical for the proper functioning of the assay. Based on the amount of $25(OH)D_3$ in the sample, there is a competitive interaction between the immobilized $25(OH)D_3$-BSA on the nitrocellulose and the $25(OH)D_3$ in the sample for binding sites on the AuNP-antibody conjugates as the sample flows through the nitrocellulose. As seen in Figure 2B, an individual with vitamin D_3 deficiency will observe a T/C ratio that is high as most binding sites on the conjugates will be empty and free to bind to the immobilized $25(OH)D_3$. Conversely, an individual with healthy levels of $25(OH)D_3$ will observe a T/C ratio that is low as most of the binding sites on the conjugates are occupied with $25(OH)D_3$ from the sample which prevents them from binding at the test line (Figure 2C).

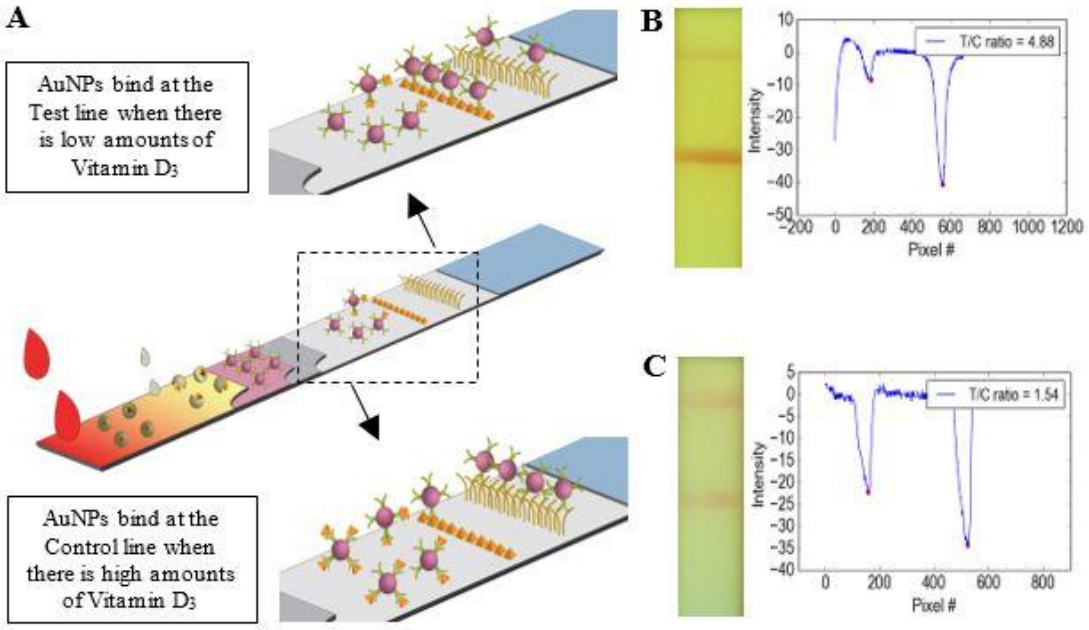

Figure 2. Vitamin D_3 Lateral Flow Assay. (A) Image and schematic of the 25(OH)D_3 strip architecture and components. **B)** Image and intensity plot of a participant with low Vitamin D_3 and high T/C ratio **C)** Image and intensity plot of a participant with healthy levels of 25(OH)D_3 and low T/C ratio.

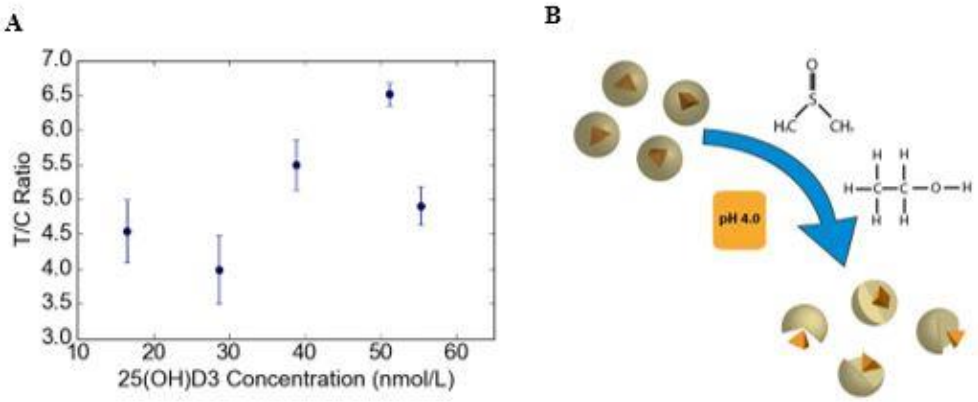

Figure 3: Elution Buffer. A) Elution of 25(OH)D_3 from binding protein with the help of organic solvents and low pH buffer and B) Calibration curve obtained from analyzing samples without the use of elution buffer. As seen, there is no relationship between [25(OH)D_3] and [T/C] without the use of the elution buffer.

2.3.4 25(OH)D3 quantification in standard solution and commercial calibrators:

In Figure 4A, we demonstrate that the T/C ratio can be correlated to a 25(OH)D_3 concentration in standard solutions. At each concentration, two strips were used and the

maximum lower and upper deviations from the average T/C values were shown. The coefficient of variation of our assay ranges from 1.7% at 100 nmol/L to 14.7% at 125 nmol/L. We then fitted a linear curve such that [25(OH)D_3] = f(T/C). We also tested the performance our assay with standard solutions that were spiked with 25(OH)D_2 in order to evaluate the cross-reactivity of the assay (inset in Fig. 4A). To verify the accuracy of the assay in serum, 25(OH)D_3 levels were also quantified in commercially available serum-based standards (ChromSystems Inc). The calibrators are based on pooled human serum and contain artificially spiked values of 25(OH)D_3 that lie in the physiologically relevant range. As seen in figure 4B, our assay is able to reliably distinguish between a deficient, insufficient and healthy sample. These standards did not require the use of the elution buffer as these samples were prepared by artificially introducing 25(OH)D_3 into the sample. The coefficient of variation of our assay ranges from 2.63% at 85 nmol/L to 11.2% at 0 nmol/L.

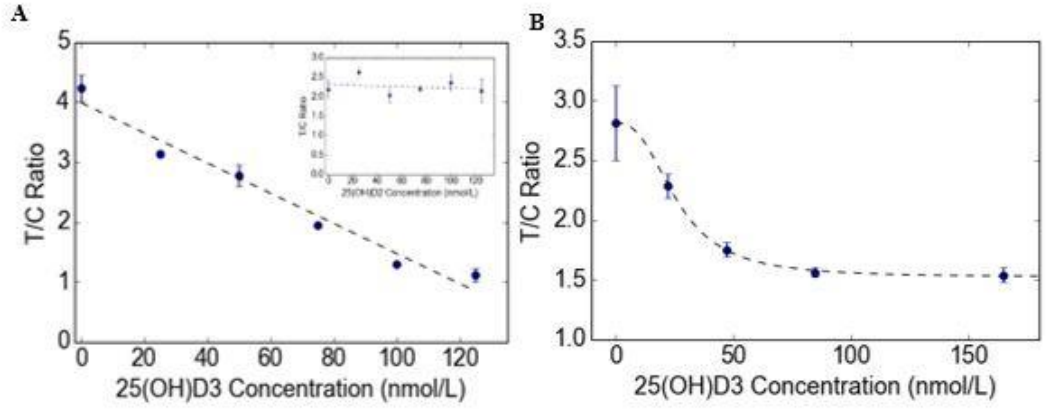

Figure 4: Calibration curve in standards. A) T/C ratios of the colorimetric signals at different 25(OH)D_3 concentration in standard buffers. T/C ratio = a[25(OH)D_3]+b, where a=-0.0251 and b =3.983. Linear logistic curve was fitted with R^2 = 0.95. The inset demonstrates a calibration curve performed with standard buffers that were spiked with 25(OH)D_2 to verify cross-reactivity. A linear logistic curve was fitted with R^2 = 0.0059 indicating no dependence of T/C ratio on [25(OH)D_2] B) T/C ratios of the colorimetrics signals at different 25(OH)D_3 concentrations in commercial serum based calibrators. T/C ratio$= d + \frac{a-d}{1+(\frac{[25(OH)D3]}{c})^b}$, where a = 2.81, b = 2.63, c = 26.2 and d = 1.52. A four-parameter logistic curve was fitted with R^2 = 0.99. At each concentration two strips were used and the maximum and minimum deviation from the average is shown as error bars.

2.3.5 Vitamin D3 deficiency testing in human serum:

Our assay was used to quantify the vitamin D_3 levels in human serum samples that were collected from a human trial to demonstrate the assay's applicability in the clinical setting (Fig 5A, 5B and 5C). Native serum samples required the use of elution buffer to separate $25(OH)D_3$ from vitamin D binding protein. As expected of our competitive type architecture, the T/C ratio for a participant with vitamin D deficiency appears to be significantly greater than that of a participant with vitamin D insufficiency. Actual serum $25(OH)D_3$ values were quantified using tandem liquid chromatography/mass spectrometry (LC/MS-MS). Figure 5B shows a ROC curve for the serum tests based on a linear calibration curve that was determined from the same batch of test strips (figure 5A). We used the DeLong method[27] to obtain an asymptotically exact method to evaluate the area under curve (auc) using 300,000 iterations with a cutoff of 50 nmol/L. A similar method was used to evaluate the performance of the assay at a cutoff of 30 nmol/L[28] that can be seen in Figure 5C. Diagnostic accuracy, defined as the proportion of correctly classified subjects to all subjects, was evaluated as 90.5% and 100% for the two cutoffs respectively. Both cutoffs are based on recommendations made by the Institute of Medicine. The root mean square error was assessed to be 5.4 nmol/L. The coefficient of variation ranged from 0.05% at 43 nmol/L to 16.6% at 57 nmol/L.

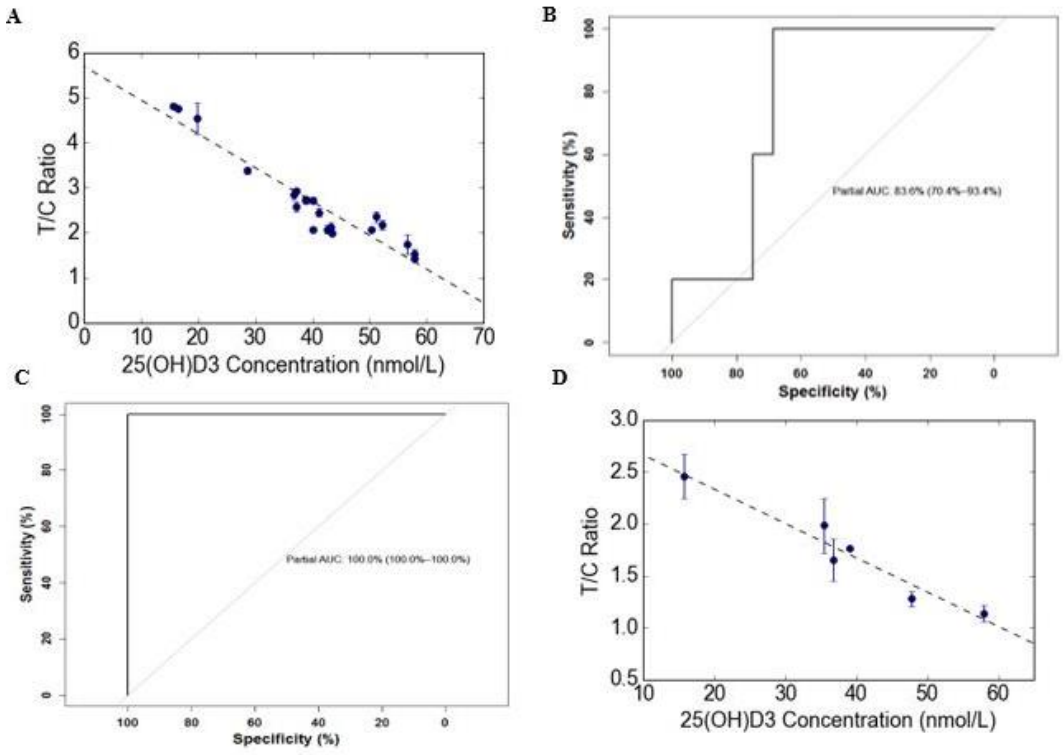

Figure 5: Analysis of human trial samples A) Linear calibration curve for 21 human serum samples with $R^2 = 0.91$. T/C ratio = a[25(OH)D3]+b where a = -0.075 and b = 5.689 B) ROC curve obtained with Delong method with n=300000 and auc 0.836 at a cutoff of 50nmol/L C) ROC curve obtained from Delong method with n=300000 and auc 1 at a cutoff of 30 nmol/L D) Calibration curve from 6 human finger stick blood samples with $R^2 = 0.94$. T/C ratio = a[25(OH)D3] + b where a = -0.033 and b = 2.9925.

2.3.6 Vitamin D3 deficiency testing in finger prick blood samples:

We used our assay to quantify vitamin D_3 levels in finger prick blood from volunteers after obtaining informed consent, as per a protocol approved by the Institutional Review Board at Cornell University. Samples were run and analyzed at the site of the trial. Figure 5D demonstrates a calibration curve for the sample set with R^2 value of 0.94. From figure 5D, it is apparent that our assay demonstrates a linear correlation between the T/C ratio and [25(OH)D_3]. Additionally, by observing the change in T/C ratio, we are able to demonstrate that our test can distinguish between a severely deficient,

deficient and insufficient participant with reasonable certainty. The coefficient of variation ranged from 0.5% at 39 nmol/L to 17.2% at 48 nmol/L.

2.4 Discussion

In this work, we demonstrate a rapid and easy to use microfluidic platform for the assessment of vitamin D status. We showed the quantification of 25(OH)D_3 in the physiologically relevant range within minutes. This was achieved by using a competitive type lateral flow assay that incorporates a novel elution buffer which separates 25(OH)D_3 from its binding protein on the strip, therefore eliminating the need for tedious sample preparation. The assay produces a colorimetric image that can be analyzed to obtain a T/C ratio that can be correlated to a concentration of 25(OH)D_3 in the sample (serum or blood). We further validate the system by quantifying levels in trivial amounts of human serum and a finger prick of blood. Given the limitations of traditional clinical diagnostic methods, our assay has the potential to make an immediate impact in the point-of-need setting as an accurate tool for the assessment of vitamin D_3 status.

Our work presented here is the first quantitative, point-of-need diagnostic test for the assessment of vitamin D_3 status and represents a critical step towards transitioning vitamin D deficiency testing out of the lab and into the hands of individuals. Unlike commercial platforms that have been developed for micronutrient testing, our test is able to process finger stick blood, denature vitamin D binding protein in situ and quantify levels of 25(OH)D_3 in the sample in a few minutes without the need for expensive equipment. These unique traits coupled with a high diagnostic accuracy (90.5%) make our test sufficient for application at the point of need. Our assay is designed specifically for assessing 25(OH)D_3 status in the deficient range (< 50 nmol/L) as this is where differentiation is most important. However, we have also demonstrated

that our test is able to reliably quantify concentrations in the complete physiologically relevant range (0 – 150nmol/L). Since our assay is unable to detect 25(OH)D_2, the quantitative ability is limited when used in settings where ergocalciferol is the preferred supplement. However, the recent uptake in vitamin D_3 supplementation suggests that our diagnostic test is practical for use in many point-of-need settings[29,30]. Given the minimal amount of expertise needed to run the assay, our test enables individuals to evaluate their own vitamin D status irrespective of their medical training or knowledge. The low cost and portability of the testing platform will also make monitoring and evaluation of the efficacy of nutrition interventions feasible in both research and programmatic settings. Furthermore, we have developed a protein elution buffer that could be adopted to improve several other diagnostic tests that require specialized sample preparation because of the presence of a binding protein (vitamins A, B_7 and B_{12}).

2.5 Materials and Methods:

2.5.1 Gold Nanoparticle Conjugation

The monoclonal anti-25(OH)D_3 IgG produced in mouse (GenScript Inc) was conjugated with 40nm Gold Nanoparticles using the InnovaCoat Gold Conjugation Kit (Innova Biosciences Ltd). For the conjugation, 0.23µg AuNP in freeze dried form was mixed with 1ug anti 25(OH)D_3 IgG in 0.01 M amine free phosphate buffer saline at pH 7.4. The anti-25(OH)D_3 IgG is attached to the surface of AuNP via lysine residues during a 15-minute incubation and the reaction was terminated by adding 0.1M tris-buffered saline (TBS) with 0.1 % Tween 20. To remove excess antibodies, DI water was added in 10 times the volume of the conjugate mixture as centrifuged at 9000 g for 10min. Upon removal of the supernatant, the final gold nanoparticle concentration was reconstituted in 0.01M TBS containing 2% BSA and the final optical density was

verified by using Spectramax 384 to measure absorbance of the conjugates at a wavelength of 530 nm. The conjugates were stored at 4ºC until use. Conjugate pads were prepared by first diluting the conjugates to roughly 0.7 – 0.8 OD (depending on application) in a conjugate buffer (2mM Borate buffer with 5% sucrose) which contained appropriate preservatives. Glass Fiber conjugate pads (EMD Millipore) with 30cmx5cm dimensions were soaked in diluted conjugate solution for 2 minutes followed by drying at 37 ºC for a minimum of 12h.

2.5.2 Vitamin D3 lateral flow assay preparation:

Hi Flow Plus 180 membrane Cards (EMD Milipore) were used as the assay platform. The membrane cards have a 2mm clear polyester film backing that contains the nitrocellulose membrane and the adhesive that allows for assembly of conjugate and sample pads. The nitrocellulose part of the assay extends for 2.5 cm in length and has a nominal capillary flowrate of 45 seconds/cm. This is the slowest flow rate offered by the manufacturers and was chosen to allow for maximum reaction time between the sample and the conjugates due to the relatively low detection range. The test and control lines were prepared by using a Lateral Flow Reagent Dispenser (Claremont Bio) to dispense 0.4mg/mL of anti-mouse IgG produced in goat and 1mg/mL of 25(OH)D_3-BSA. The two lines are separated by 3mm and have line widths of 1mm. These lines were dispensed using the Legato 200 Dual Syringe Pump (Claremont Bio) at 6.7µL/min. Once the reagents were dispensed, they were dried for a minimum of 12 hours at 37ºC. The final assay was assembled by first applying the spacer pad onto the bottom of the nitrocellulose portion with 2-3mm overlap followed by a dried conjugate pad. The sample pad, which is the final component, varies based on the sample that is to be tested. Cellulose pads (EMD Milipore) were used for serum samples and FR1 blood filtration membranes (MDI membrane technologies) were used for blood samples. In both cases,

the sample pad was attached below the conjugate pad with 2mm overlap. The FR-1 membrane has a thickness of 0.35 mm and capacity of 30µL/cm^2 and measured to be 30 cm x 2.5cm while the Cellulose pad measured to be 30cm x 1cm. Another cellulose fiber sample pad was attached at the top of the nitrocellulose card to serve as an absorbent pad to collect any waste from the assay. The assembled assay was then cut into 4mm strips using a rotary paper trimmer. The strips were then kept sealed in a plastic container and wrapped in aluminum foil in a humidity controlled chamber (Secador) for a few days to prevent adverse effects of exposure to varying temperature and humidity. Test strips remain integral for up to several weeks while stored in these conditions. However, their shelf life can be extended up to a year if they are sealed in light safe mylar pouches and stored at room temperature.

2.5.3 Elution buffer preparation:

A combination of organic solvents and low pH buffers was used to ensure the separation of vitamin D binding protein and 25(OH)D_3 on strip. We mixed 4.7 parts of 1:1 mixture of Dimethyl sulfoxide (VWR) and Pure Ethanol (Acros Organics) with 1 part of pH 4.0 acetate buffer (VWR). In the case of finger prick blood testing, 4µL of this mixed buffer was added to the area of overlap between the blood filtration membrane and the conjugate pad to allow for the filtered serum to interact with the elution buffer prior to the reaction with the conjugates. Elution buffer cannot be added directly to whole blood as the organic solvents cause lysing of blood cells. As for serum, the same amount of elution buffer was mixed in with the sample in a plastic 1.5 mL micro-centrifuge vial prior to applying the sample to the strip.

2.5.4 Vitamin D3 test strip protocol and human trials:

Capillary tubes were used for the collection of constant amount of blood from the participants. First, 4µL of elution buffer was pipetted onto the area of overlap between the sample pad and the conjugate pad. This allows for the filtered serum to interact with the elution buffer prior to the conjugates. Elution buffer is added prior to the interaction of the sample with the AuNP-anti 25(OH)D_3 conjugates to avoid affecting the performance of the gold nanoparticles. Nanoparticle aggregation was observed when the conjugates are mixed directly with elution buffer. Additionally, adding elution buffer to the sample prior to incubation reduces the adverse effects of the elution buffer on the conjugates. After allowing for 4 minutes for the sample to filter into serum, 15 µL of running buffer is added to flow the sample and elution buffer mixture into the conjugate pad. After allowing for an additional four minutes of incubation, 25 µL of running buffer is added to start the flow onto the nitrocellulose membrane. At this point, the user inserts the cartridge into the imaging device. The imaging device automatically images the diagnostic test when the test and control lines are fully developed.

The human trials were approved by the Institutional Review Board for Human Subjects at Cornell University and carried out in accordance with their regulations. Informed consent was obtained from all participants prior to testing. For the trial, the participants were subjected to a finger prick (UniStik) for a drop of blood which was collected using a capillary tube and dispensed onto the sample pad. A trained and certified phlebotomist then drew 5mL of blood via venipuncture which was used for tandem mass spectrometry analysis. Following 1-hour incubation at room temperature, serum was separated by centrifugation at 2000 g for 10 min. Serum 25(OH)D levels were characterized using tandem mass spectrometry (LC/MS-MS).

2.5.5 TIDBIT and image processing:

Test strips were imaged using a portable imaging device designed specifically for colorimetric detection and quantification. The device consists of a 5-megapixel 1080p HD CMOS camera (Rasbperry Pi), focusing lens and LEDs (Thorlabs Inc), raspberry Pi computer board, rechargeable lithium ion battery pack (Adafruit Industries) and slide out cassette tray, all surrounded by a 3D printed light tight container. Once the cassette is inserted into the imaging device, it is automatically imaged and processed using a custom python script.

CHAPTER 3

H.E.R.M.E.S: RAPID BLOOD-PLASMA SEPARATION AT THE POINT-OF-NEED*

3.1 Abstract

The global healthcare landscape is experiencing increasing demand for CLIA-waived testing facilities that offer diagnostic capabilities at lower costs and greater convenience than traditional laboratory testing. While several new diagnostic tools have emerged to fulfill testing requirements in these environments, centrifuges have been stymied from transitioning to the point-of-need as the US Food and Drug Administration (FDA) classifies them as mostly unsuitable for use in CLIA-waived environments. Limitations in sample processing capabilities adversely affects the ability for CLIA-waived testing environments to offer a broad testing portfolio and present-day diagnostics are bottlenecked by the requirement for centrifugation. Here we present the High Efficiency Rapid Magnetic Erythrocyte Separator (H.E.R.M.E.S), a rapid low-cost technology that can perform the separation of red blood cells from plasma at a fraction of the time and cost of that of a centrifuge. We demonstrate that H.E.R.M.E.S is able to obtain highly-pure plasma (greater than 99.9% purity) at less than 2 minutes per test. Further, we detail that it is an easy-to-use method capable of being incorporated with present-day diagnostic technologies and prove that it is superior to existing alternatives to centrifugation by validation with a ferritin lateral flow test. H.E.R.M.E.S is a suitable [1] alternative for centrifugation in point-of-need settings and aims to facilitate the decentralization of commercial blood testing

*Reprinted with permission from Vemulapati, S. and Erickson, D. *Lab on a Chip* ***18****, 3285–3292 (2018).*

3.2 Introduction

The US blood testing market is estimated at $20 billion and is expected to increase to $30 billion by 2030[29]. This predicted growth stems from an increasing demand for CLIA-waived testing environments, such as Urgent Care and Minute Clinics, that offer diagnostic capabilities at lower costs and greater convenience than conventional laboratory testing. CLIA-waived clinics embody a shift in the healthcare landscape towards decentralization and higher accessibility of medical testing. The separation of unwanted cellular material is critical for the accuracy and reliability of many molecular diagnostics tools[30], for example many blood tests require that plasma is separated from red blood cells prior to analysis. In commercial blood testing laboratories, centrifuges are almost exclusively employed to perform separation and is a key first step to facilitate accurate quantitative diagnostics[31]. However, the US Food and Drug Administration (FDA) classifies centrifuges as 'moderately' complex devices that are unsuitable for use in CLIA-waived environments[32]. This constraint has bottlenecked the translational ability of diagnostic technologies as centrifuges are unable to adapt for use at the point-of-need and are becoming increasingly obsolete in a landscape that is seeking the further decentralization of testing services.

Passive filtration membranes are a solution to perform cell separation at the point-of-need and are often used with lateral flow assays[33]. Enabled by capillary action, the membranes operate on the principle of selectively preventing particles of a certain size from flowing through them. While inexpensive and easy to manufacture, the performance of these membranes is marred by inconsistencies in separation caused by clogged pores. Inconsistencies manifest themselves as variability in amount of plasma that is obtained during each run which deters the performance of quantitative lateral flow tests. Immunochemistry is sensitive to a variation in amount of sample that is used for analysis[34,35]. Additionally, the recovery rates of these methods is low[36] (less than

30% of available plasma) which presents a barrier for analysis of analytes at low concentrations and sizes[37].

Several microfluidic approaches have been demonstrated in literature that achieve high levels of separation. These methods can be broadly classified into "active" and "passive" techniques[38]. Active techniques employ an external field (acoustic, electric or magnetic) that is used to align or immobilize the blood cells so as to enable the plasma to be separated in a continuous flow format. Passive methods typically separate the cells using hydrodynamic effects or separating pillars using cleverly designed and intricate microfluidic fabrication architecture[39–41]. While these techniques have been excellent demonstrative proof-of-concepts, they lack the ability to be commercialized as microfluidic fabrication is a highly involved and expensive process that lacks scalability[42]. Further, in the case of active methods, the complex designs are often too cost-ineffective to integrate into existing microfluidic methods rendering them impractical for use at the point-of-need[37]. To address the high cost and lack of accessibility, many researchers have used common household items and toys like salad spinners and egg beaters to achieve plasma separation[43–45]. These designs were cleverly engineered to simulate centrifugation but are not robust enough to operate in point-of-need clinical settings. There is a need for low-cost technologies that can offer highly efficient blood-plasma separation at the point-of-need with high reliability and efficiency. A 'simple' method would further enable present day diagnostics to transition for use at the point-of-need[46–49] and enable the decentralization of blood testing services. In this paper we detail the design and principle of the High Efficiency Rapid Magnetic Erythrocyte Separator (dubbed H.E.R.M.E.S), a portable low-cost system that enables the separation and extraction of red blood cells from plasma within 2 minutes. H.E.R.M.E.S uses functionalized magnetic beads to capture and separate red blood cells and achieves near perfect separation, rivaling the efficiency of that of a commercial

centrifuge while using inexpensive raw materials. H.E.R.M.E.S employs a standalone protocol that does not require the use of any specialized lab equipment such as pipettes. We demonstrate the efficacy of H.E.R.M.E.S with the help of human samples, and further prove that H.E.R.M.E.S improves the performance of existing lateral flow assays in comparison to commercially available filtration membranes.

3.3 Results

3.3.1 H.E.R.M.E.S Device Design Landscape

H.E.R.M.E.S has been designed with a specific intention of being easy-to-use. The process involves three main phases: capture, separation and extraction. In order to obtain separated plasma, the user need only follow three steps (as outlined in Figure 6a), i) collect the sample (typically with a finger-stick) and load the sample in a test tube precoated with functionalized magnetic beads, ii) place sample in H.E.R.M.E.S and wait for 2 minutes, iii) remove sample and extract plasma using a capillary tube. Once the sample has been extracted, the sample can be used for further analysis or stored for future use. The portable benchtop device itself consists simple onboard electronics to enable automation (Figure 6d). H.E.R.M.E.S employs a small linear solenoid that actuates a magnetic field in a specific direction with respect to the sample to create a mixing effect. This ensures that the beads are able to capture the erythrocytes in the sample. The device occupies a small footprint and can be powered by any standard electrical outlet. Once the device is plugged in, the actuation starts automatically and proceeds for 90 seconds. After 90 seconds, the solenoid turns off and the magnetic beads are concentrated by the magnet on one side of the sample holder. The user then employs a small capillary tube to uptake the separated plasma. While the current iteration requires the use of an outlet, it can be easily re-engineered to include a portable battery pack instead. H.E.R.M.E.S was specifically designed to enable sample processing in

point-of-need settings and was designed for semi-autonomous operation to minimize the need for manual intervention by the user.

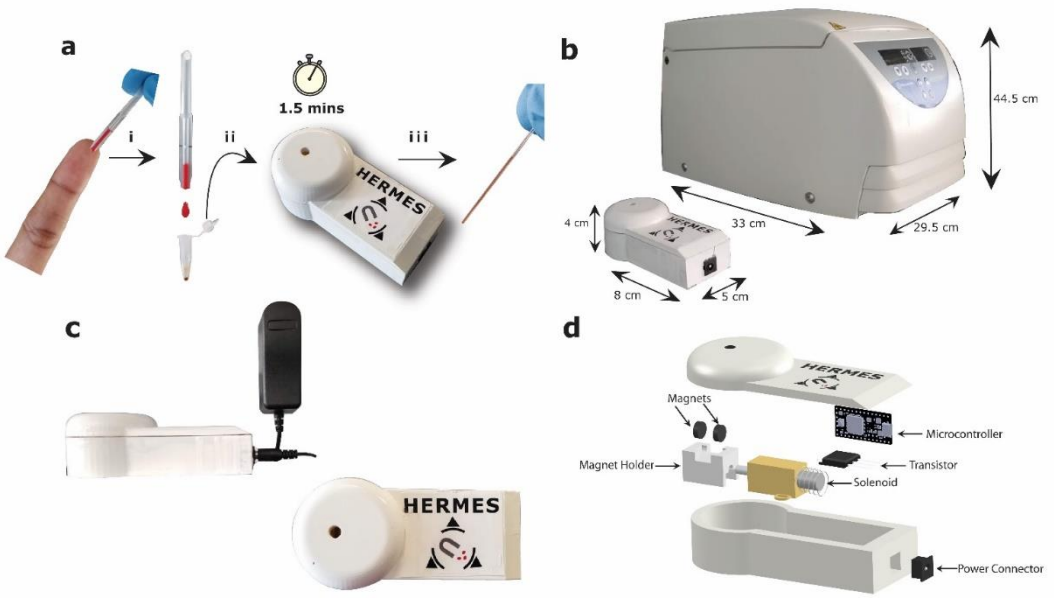

Figure 6: a) Using H.E.R.M.E.S involves 3 simple steps i) collect and load the sample in a test tube precoated with functionalized magnetic beads, ii) place sample in H.E.R.M.E.S and wait for 90 seconds, iii) remove sample and extract plasma using a capillary tube. b) Size comparison of H.E.R.M.E.S against a standard laboratory centrifuge (Fisherbrand accuSpin Micro 17) c) Side and top profile of the portable benchtop device respectively and d) exploded view of H.E.R.M.E.S showing its internal components.

3.3.2 Magnetic bead capture of erythrocytes

Magnetic bead based capture has been adopted several biological applications such as DNA extraction, peptidome assessment and immunocapture[50–52]. The technique is particularly useful for capturing a small amount of analyte as the beads can be concentrated to yield a higher limit of detection[53]. H.E.R.M.E.S tackles the opposite problem: a single microliter of human blood can contain up to 6 million blood cells. This resulted in a significant challenge as it was necessary to capture all the erythrocytes in the sample without the need for dilution. At first glance, it would appear a simple assessment of the binding capacity of the magnetic beads would be sufficient in order determine the minimum number of

beads required to capture all the blood cells in the sample. A “brute force” approach as such would be appropriate for separation but would suffer from a lack of scalability. Further, this approach would have a fragile dependence on the sample size with a cost-scaling directly proportional to the number of cells that would need to be captured. In order to maintain a cost-effective scaling principle, H.E.R.M.E.S uses an aggregation agent that groups red blood cells together during the capture phase, thereby reducing the effective number of cells that need to be captured (See Figure 7). By aggregating the cells prior to the capture, we demonstrate an approximate 2000-fold increase in binding capacity of the beads using this aggregation agent. H.E.R.M.E.S is unique in comparison to previous works in literature that employ aggregation enhanced capture as it is performed in an easily accessible format that does not require specialized filtration paper or microfluidic setup[54,55]. Our estimations reveal that on average, one bead is able to capture up to 100 cells due to the aggregation effect. Approximately 5.4 mg of blood cells are captured with close to a tenth of the amount of beads.

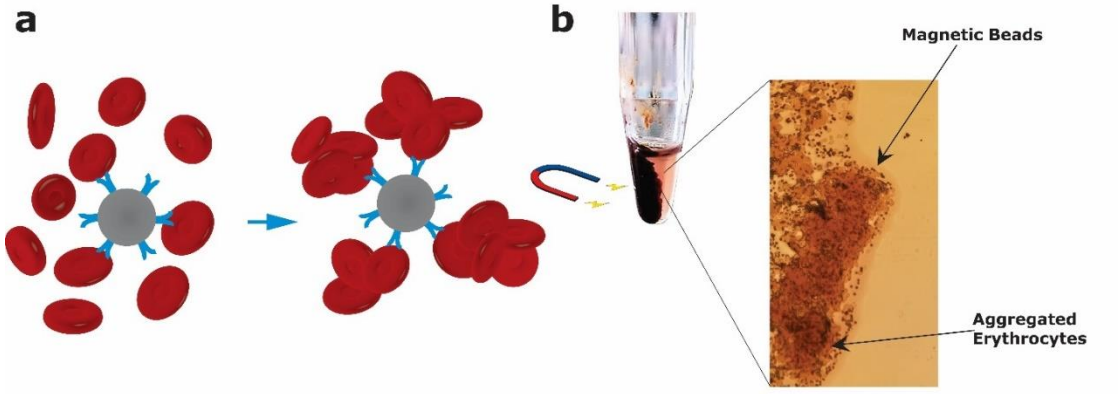

Figure 7: a) Effect of aggregation of blood cells prior to capture and b) Separation of plasma from captured red blood cells with application of a magnetic field as seen under a microscope

3.3.3 Evaluation of H.ER.M.E.S using human samples

We used H.E.R.M.E.S to process blood samples from 15 individuals and analyzed the plasma obtained after extraction (Table 1). We demonstrate an average purity greater than 99.9% (less than 20 cells/µL counted) and an average extraction time of 108 seconds to obtain 90% of the available plasma. H.E. R.M.E.S demonstrates a high efficiency to capture and separate red blood cells irrespective of blood type and hematocrit levels (See Appendix A). To further demonstrate the ability of aggregation to enhance the capture rate, we used H.E.R.M.E.S to separate erythrocytes in artificially spiked blood samples that have abnormally high hematocrit (Figure 8). We hypothesize that the aggregation effect scales non-linearly with an increase in the number of red blood cells. The high concentration of blood cells decreases the interaction space leading to effective binding in these samples. H.E.R.M.E.S can perform reliably with an increase in red blood cells and is able to obtain highly pure plasma regardless of the number of blood cells. Factoring in the cost of the aggregation agent and the beads, we expect H.E.R.M.E.S to cost less than $2 per separation test (See Appendix A).

Table 1: Data collected from testing 15 human blood samples with varying ages, hematocrits and blood types. A starting volume of 40 µL was used for each test. Samples were run in duplicate and the standard deviation is reported. Average volume of uncontaminated plasma obtained from centrifugation was 18.2 µL. All samples were purified using 0.625mg of magnetic beads and 200µg of aggregation agent.

Average Purity of Obtained Plasma	**99.95 ± 0.05%**
Average Time for Extraction	**108 ± 21 seconds**
Average Volume Obtained	**17.2 ± 1.96 µL**

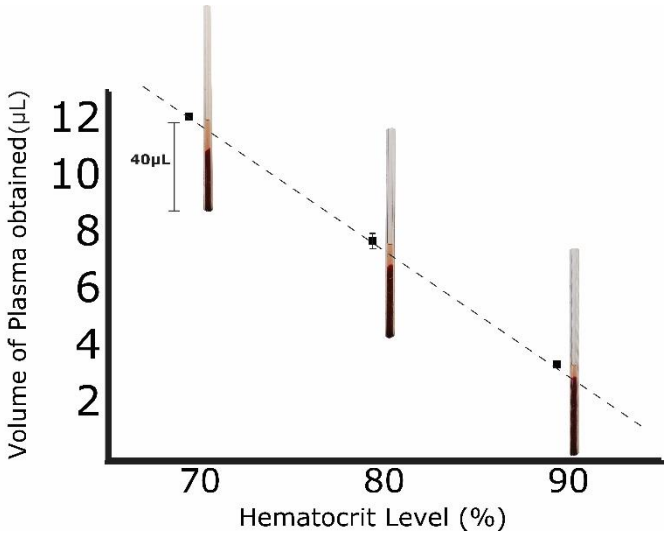

Figure 8: Separation of Plasma from human samples with artificially high hematocrit values. Each sample was tested in duplicate and the standard deviation for each sample set is indicated with error bars (n=2). An average purity of 99.9% was obtained in these samples.

3.3.4 Quantifying the effect of aggregation on performance

Aggregation reduces the number of effective targets that need to be captured to obtain highly pure plasma. To understand the dependence of the aggregation capabilities on separation performance, we tested the cell capture rate with varying levels of aggregation agent. The cell capture rate was indirectly inferred by calculating the purity of the plasma obtained after separation. We then compared the purity of plasma obtained using different sample volumes to assess the scalability of the technique. As seen in figure 9, it can be noted that a concentration of about 3.5mg/mL of aggregation agent is sufficient to obtain plasma of high purity (greater than 99%). We also observe a non-linear relationship wherein the binding capacity is amplified several-fold as the amount of agent is increased. We expect the curve to be pushed further out in the regime where the concentration of the aggregation agent is low. However, there exists a critical concentration that creates the level of aggregation necessary to obtain highly pure plasma (greater than 99%). In contrast, we also studied the effect of increasing the

number of magnetic beads on performance and noted that the amount of beads does not significantly affect the separation of performance.

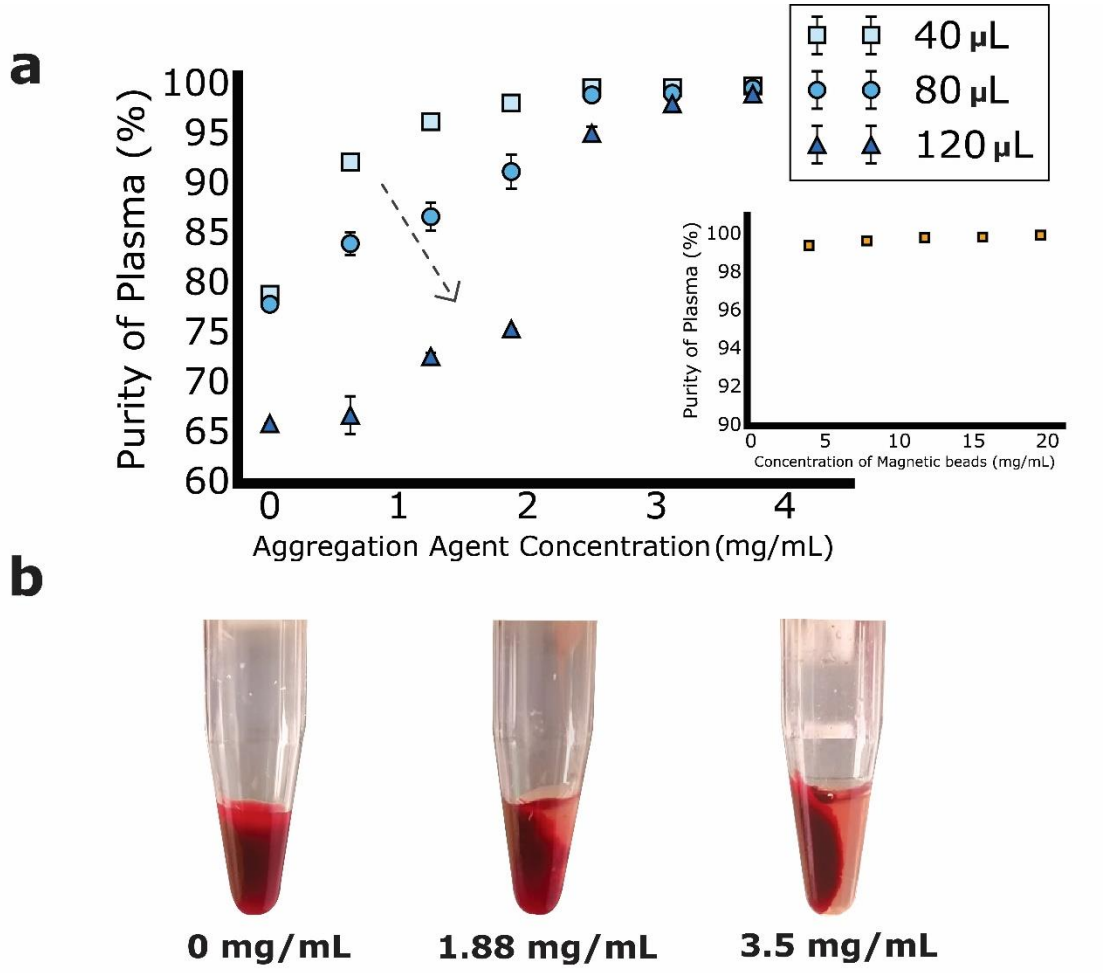

Figure 9: a) Plot showing the effect of the aggregation agent on performance of H.E.R.M.E.S. Three different sample volumes were used *as noted in the legend*. A non-linear relationship is observed between the amount of blood cells and the amount of aggregation agent required to capture them. An average of 34 µL and 53 µL of total recovered plasma were obtained in the cases of samples tested using 80 and 120 µL volumes. Standard deviation for each sample is indicated with error bars. (n=2). The inset shows that the concentration of magnetic beads does not affect the performance significantly. b) Images of separated plasma at three different aggregation agent concentrations. A concentration of around 3.5mg/mL is optimal to obtain highly pure plasma.

3.3.5 Integration with existing diagnostic testing platforms

We demonstrate the ability of H.E.R.M.E.S to augment the performance of present-day diagnostics by incorporating the technology with lateral flow test strips – a common diagnostic platform often implemented for use at the point-of-need. Ferritin lateral flow strips previously described by Srinivasan et al[56] were tested using 10 human blood samples. We compared the performance of H.E.R.M.E.S against commercially available filtration paper (MDI). A calibration curve was built with a linear trendline fit to compare the performance of the two test cases (Figure 10). In general, we observed that H.E.R.M.E.S leveraged higher quantitative power from the regression model used in each of these cases. ROC curves were plotted using the Delong method[27] and a difference in performance was established. Further, as seen in figure 5 a higher slope (46%) was noted for test strips that incorporated plasma obtained from H. E.R.M.E.S indicating greater quantitative ability across the concentration range of interest. More importantly, H.E.R.M.E.S was able to demonstrate a significantly reduced average coefficient of variation (6% vs 21%) further proving that it is capable of advancing the performance of point-of-need testing platforms.

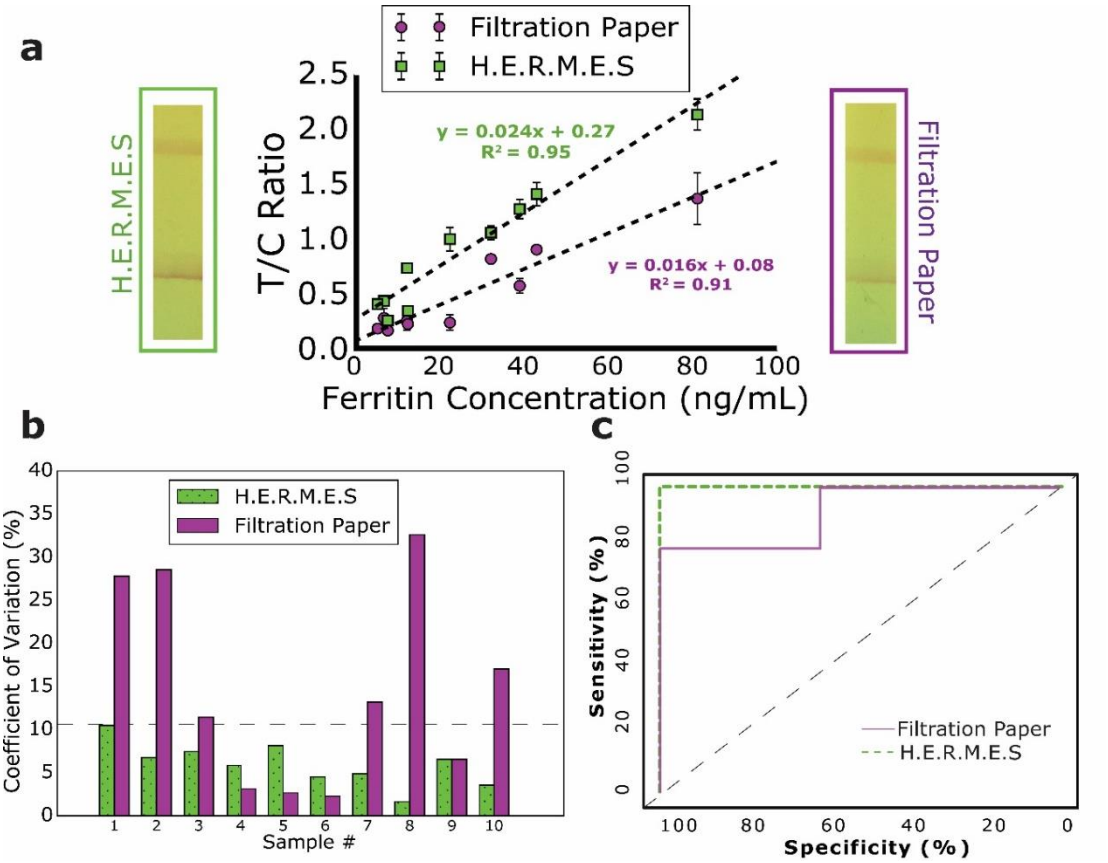

Figure 10: a) Plot comparing the performance of plasma obtained from H.E.R.M.E.S *and* commercially available filtration paper. A starting volume of 40µL was used for each test and 15µL of plasma was used for the strips that were used with H.E.R.M.E.S. The pictures on the left and right side of the plot are images of test strips run using plasma obtained from H.E.R.M.E.S and filtration paper respectively. In general, we note a higher T/C ratio for all the samples that used H.E.R.M.E.S for separation. Further, we observe a higher coefficient of determination R^2 and a sharper slope in the case of samples processed with H.E.R.M.E.S. The standard deviation of each sample (n=2) is indicated by error bars. b) Comparison of the mean coefficient of variations (CV = standard deviation/mean *100) between the two types of plasma. The CV of all samples from H.E.R.M.E.S was lower than 10%. c) Comparison of the ROC curves (generated using the Delong method). The a.u.c from samples purified by H.E.R.M.E.S was 1 and the a.u.c from filtered samples was 0.789.

3.4 Discussion and Conclusion

H.E.R.M.E.S leverages the elementary concept of magnetic separation to carry out a challenging process of separating unwanted cellular material from a sample. The method was specifically designed to be low-cost, rapid and minimally complex. The

system was designed to allow for maximal automation and minimal intervention from the user while maintaining a low-cost. These characteristics make H.E.R.M.E.S a promising alternative to the traditional lab centrifuge in settings where a centrifuge cannot operate, whether due to regulatory constraints or resource limitations. Further, while we validated H.E.R.M.E.S with a commonly available point-of-need testing platform (lateral flow tests), it is universal and can be used to simplify purification for virtually any diagnostic test that requires plasma or serum as an input. While there are a handful of sophisticated commercial platforms that are capable of performing immunoassay chemistry without the need for separating red blood cells, H.E.R.M.E.S will enable the use of standard diagnostic techniques in low-resource settings where other alternatives are not feasible. Further, the high recovery rate (>90% of available serum), the low time for recovery, the low cost and ease of use of the system make it superior to solutions that have been demonstrated in literature. [33,36,57]

H.E.R.M.E.S has the potential to impact the blood testing industry due to its ability to offer the separation efficiency of a centrifuge at a fraction of the time and cost. H.E.R.M.E.S seeks to facilitate the implementation of present-day diagnostic tools at the point-of-need by integrating into CLIA-waived testing environments where centrifuges are currently unable to operate. H.E.R.M.E.S can enable rapid front-end sample processing to help prevent loss of sample quality in these environments by ensuring that all red blood cells are removed prior to clinical chemistry testing. We envision H.E.R.M.E.S having immediate applicability in advancing molecular diagnostics such as PCR to the point-of-need as it can integrate easily into existing methods for translational PCR. Particularly, the isolation of white blood cells makes an interesting use case for infectious disease detection[58,59] and genetic sequencing[60]. In addition to being highly scalable due to the low cost of raw materials that are involved in fabrication, H.E.R.M.E.S is able to perform highly efficient blood plasma separation

within 2 minutes at less than $2 per test and is suitable for use in resource-limited settings. While the current iteration of H.E.R.M.E.S is only capable of accommodating one sample, we envision that a future prototype will possess parallel sample processing capabilities as the underlying technique is highly scalable. Further, the stand-alone system is easy to use and can be adopted by users irrespective of their prior medical training making the H.E.R.M.E.S a unique method to perform blood-plasma separation at the point-of-need.

3.5 Materials and methods

3.5.1 Preparing Magnetic beads:

Magnetic beads (ProMag HP, Bangs Labs) suspended in a 50mM MES Buffer were conjugated to a Anti Red Blood Cell antibody (Rockland Antibodies) by incubating the sample in an end-over-end mixer for 12-15 hours. After conjugation, the supernatant was removed and replaced with a storage buffer (10mM Tris Buffer, pH 8, 0.05% Bovine Serum Albumin, 0.05% Proclin 300). The beads were stored at 4-8°C in liquid form and are stable up to several months. Prior to testing, 325 µg of beads and 200µg of antibody were loaded in a single PCR tube (Eppendorf) and dried in a vacuum centrifuge (Eppendorf Vacufuge 5301) for 30 minutes. The antibody is added separately to induce clumping of the red blood cells to reduce the number of effective targets during the capture process. Dried beads were then used for tests or stored at 4-8°C. The dried beads demonstrated a shelf life of up to three months when sealed in a dark container.

3.5.2 H.E.R.M.E.S benchtop unit:

A small portable benchtop unit was designed in Sledworks and printed using a Objet 3D printer. The device itself consists of a microcontroller (Teensy 3.2, Sparkfun), a few

transistors and a 12V actuating solenoid (Adafruit Industries). Two circular neodymium magnets (K&J Magnetics) were mounted on a 3D printed holder and attached to the solenoid. The device also has a power input jack that can be connected to standard 12V, 0.5A wall power supply.

3.5.3 Analysis of Plasma:

Upon separation of plasma from the red blood cells using H.E.R.M.E.S, a capillary tube (Microcaps, Drummond Scientific) was used to extract the serum from the sample and transferred into another test tube. Once transferred, the serum was diluted 5 times and mixed in a 1:1 ratio with trypan blue stain. Once stained, the serum was loaded into a disposable hemocytometer (C-Chip, Cyto Diagnostics) and cell counting was performed under a bright field microscope. The number of cells counted were then used to estimate the purity of the plasma obtained.

3.5.4 High Hematocrit Samples:

Blood samples with abnormal hematocrits were prepared with type O human red blood cells suspended in alsever's solution (Innovative Research). The blood cells were spun down and concentrated in a centrifuge and resuspended to abnormally high hematocrit values (70,80 and 90%)

3.5.5 Lateral Flow Test:

Ferritin strips were manufactured similar to work mentioned in Srinivasan et al. We prepared two batches of test strips with blood filtration membranes (Type FR-1(0.35) MDI membrane technologies) used as a sample pad. The FR-1 is a passive forward flowing filtration membrane that has a thickness of 0.35 mm and capacity of 30 $\mu L/cm^2$. 10 human blood samples (Innovative Research) were then used for testing. For the strips that used the filtration membranes, a 3-minute incubation period was added at the

beginning of the test to allow the plasma to filter through the membrane. This was followed by the application of 40uL of running buffer to start the test. For the test cases that used plasma from H.E.R.M.E.S, the test was immediately started by using a 15µL capillary tube to apply the plasma onto the sample pad followed by application of 40µL of running buffer. We note that these test strips could also have been used as a dipstick format, wherein the sample pad is dipped in the sample holder to start the test. After 30 minutes, the test strips were imaged using the TIDBIT (previously mentioned by Lu et al[61]) and a calibration curve was built using custom python code. Actual ferritin values were obtained using a SIEMENS Immulite1000 immunoassay analyzer.

3.6 Acknowledgements

Sasank Vemulapati would like to thank Vicky Simon in the College of Human Ecology at Cornell University for analyzing the true ferritin values of the sample. They would also like to acknowledge that the device was 3D-printed at the Cornell NanoScale Science and Technology Facility (CNF). **Funding**: Part of this work was funded with NSF award #1343058 and a Cornell University College of Engineering Scale Up and Prototyping Award.

CHAPTER 4

cAST: CAPILLARY-BASED PLATFORM FOR REAL-TIME PHENOTYPIC ANTIMICROBIAL SUSCEPTIBILITY TESTING

4.1 Abstract

Antibiotic resistance is recognized as one of the greatest threats to public health. Antibiotic resistant pathogens affect nearly 2 million people a year in the US alone and creates an estimated $34B burden on the healthcare system. The rise in occurrence of resistant organisms can be attributed to a combination of over-prescription of antibiotics and a lack of accessible diagnostic methods. Delayed diagnosis is the primary reason for increased clinical risk and diagnostic methods that can enable a quick and accurate result are highly desirable to help enable effective treatment. This is particularly true for clinical situations at the point-of-care where access to state of- the art equipment is scarce. We present here cAST, a unique approach that offers accelerated assessment of antibiotic resistance in a low-cost and simple testing format. cAST delivers an expedited time to readout by means of colorimetric assessment of a resazurin dye that is incubated with the pathogen in a small capillary form factor. cAST was built using a combination of off-the-shelf and custom 3D printed parts, making it extremely suitable for use in resource-limited settings. We prove that growth of bacteria in cAST is approximately 25% faster than in a conventional well microplate and further validate the diagnostic performance with 5 clinically relevant infectious organisms. We demonstrate that cAST

can deliver accurate AST results within 4-8 hours and discuss the potential for the underlying technology to be implemented into conventional optical AST assays.

4.2 Introduction

In recent years, the emergence and increasing occurrence of antimicrobial resistance (AMR) is a serious public health concern that places a substantial burden on the healthcare system. Antibiotic-resistant infections are associated with longer hospital stays, poorer clinical outcomes, and increased healthcare costs [62]. The Center for Disease Control (CDC) estimates that more than two million antibiotic-resistant infections occur in the US each year, resulting in at least 23,000 deaths, $20 billion in excess direct healthcare costs, and $35 billion in lost productivity [63]. The threat of AMR is exacerbated by the over-prescription of broad-spectrum antibiotics as well as the lack of new antibiotics from the pharmaceutical industry [62]. The empirical prescription of antibiotics induces selective pressures that promote the development of antibiotic resistant organisms. As a result, diagnostic methods that can eliminate diagnostic uncertainty and enable evidence-based treatment form one of the most effective ways to curb antibiotic misuse and in turn the development of resistant organisms [64].

To facilitate the appropriate prescription of antibiotics, common methods of assessing the antimicrobial susceptibility of bacterial isolates include broth dilution, disk diffusion, and use of automated instrumentation [65,66]. In broth dilution, bacterial inoculums are cultured overnight in tubes of liquid growth medium supplemented with different concentrations of antibiotics. Following incubation, visual inspection of the tubes for turbidity, which is evidence of bacterial growth, is conducted to determine the minimal inhibitory concentration (MIC). Quantitative determination of MIC is one of the primary advantages of broth dilution, but the technique is limited by the relatively large quantities of reagents required. In disk diffusion, bacterial inoculums are cultured

on an agar plate with paper antibiotic disks placed on the surface. Following an incubation period of 16-24h, the zones of growth inhibition around each antibiotic disk is measured and compared to known criteria for a qualitative susceptibility assessment (susceptible, intermediate, or resistant). Disk diffusion has the advantages of being simple and low-cost but is qualitative and open to subjective interpretation of results [67]. In automated microdilution methods, incubation and optical detection systems are combined and used to detect bacterial growth in the presence of antibiotics in multi-well microdilution format, although manual preparation of inoculums is typically required beforehand [67]. While automated instrumentation can be leveraged to simplify workflow and enable real-time measurements, the high cost of the instruments and associated consumables limits their accessibility for use in point-of-care applications and resource-limited settings. Accessible antimicrobial susceptibility testing (AST) is crucial as evidence shows that each hour delay in proper antibiotic administration increases the risk of mortality in patients with severe sepsis [68].

Many alternatives to existing AST methodologies have been developed [69]. Examples of genotypic and phenotypic methods include tests based on resistance gene detection [70], microscopy [71,72], colorimetric detection [73,74], and microfluidics [75–78]. Because genotypic methods only determine the presence or absence of a resistance gene, phenotypic AST is needed to determine the actual susceptibility profile of an organism [79]. In phenotypic methods, speed of growth is fundamentally limited by the replication speed of the target organism; however, the sensitivity of growth detection can be enhanced with the use of colorimetric indicators. For instance, resazurin, a redox indicator that undergoes irreversible color change in the presence of metabolically active bacterial organisms, has been shown to increase sensitivity of microbial growth detection compared to turbidity alone [80]. Despite the number of innovations in this area,

the specialized training, instrumentation, and/or fabrication that many alternative AST techniques require have created barriers to clinical adoption.

In this work, we developed a novel capillary-based Antimicrobial Susceptibility Testing (cAST), a platform composed of a mix of custom and off-the-shelf components combined to enable phenotypic susceptibility testing in real-time. Our platform employs metal capillary tubes along with a resazurin dye to enable accelerated detection of bacterial growth by means of spectral measurements of sample volumes that are significantly smaller than what is needed to achieve reliable measurements in 96/384 well plates. We demonstrate that our system can detect bacterial growth and determine antibiotic susceptibility for several clinically relevant organisms within 4-8 hours of incubation. Our platform is an accessible alternative to conventional automated AST and its simplicity makes it well-suited for use in resource-limited settings.

4.3 Materials and Methods

4.3.1 Comparing growth in capillary tubes vs. microwell

To examine the impact of incubation format on bacterial growth in small volumes, bacterial incubation inside capillary tubes was compared to incubation inside wells of a 384-microwell plate. Using the same dilution steps described in detail in the susceptibility testing section, *Escherichia coli* ATCC 25922 overnight culture was diluted to a starting concentration of 5×10^5 colony-forming units per milliliter (CFU/ml) in cation-adjusted Mueller-Hinton broth (CAMHB, Becton Dickinson) and supplemented with 10% v/v of three different colorimetric indicators separately: phenol red (MilliporeSigma), bromomethyl blue (MilliporeSigma), and resazurin (PrestoBlue, Thermo Fisher). For all three colorimetric indicators, metabolically active bacteria induce color change in the media over time, which can be quantified through measuring

sample absorbance. By testing three colorimetric indicators and two sample incubation formats, we wanted to determine which combination yields the fastest detection of growth. 15µl volumes of each dye-supplemented culture were loaded into multiple capillary tubes of size 65 mm × 0.0382 in. × 0.0276 in. (L × O.D. × I.D., Drummond Scientific) via capillary action and wells of a 384-microwell plate (VWR) via pipetting. The 15µl volume was selected to ensure even coating of the well bottoms for consistent absorbance measurements. Loaded capillary tubes and the master microwell plate were incubated at 37°C. In one-hour interval between hour 0 and hour 1, 30 min. intervals between hour 1 and hour 2, and 15 min. intervals between hour 2 and hour 4, sample absorbance in the 350nm – 650nm range with 1nm resolution was measured using a SpectraMax Plus 384 microplate reader. For each measurement, capillary and microwell samples containing each of the three colorimetric indicators were transferred to a new 384-microwell plate in duplicate along with dye-supplemented CAMHB without bacteria as the negative controls. The difference in peak absorbance (peak shift) between a test sample and negative control sample was used as a quantitative indicator of bacterial growth. In a separate experiment, bacterial growth inside capillary tubes with different inner diameters 0.45mm, 0.70mm., and 0.76 mm) was quantified using the same spectroscopic approach.

4.3.2 cAST platform design and operation

The cAST platform consists of the following components: custom motor mount/sample holder, optical coupler, LED holder, and commercially available stepper motor, microcontroller, capillary tubes, and portable spectrometer. Custom device parts were designed in SolidWorks and 3D printed using an Objet 3D printer. The motor mount/sample holder houses a bipolar stepper motor (SparkFun Electronics) that drives the optical coupler during data acquisition as well as 1/16 in. stainless steel capillary

tubes (Supelco) that hold the samples. The optical coupler enabled precise alignment of a 400um fiber-optic patch cable (Edmund Optics) with the capillary tubes. The patch cable was connected to a portable spectrometer (Ocean Optics HR2000) that was used for spectral intensity measurements of samples. The LED holder was fixed with 10 high-power white LEDs (Lite-On Inc) that served as the light-source for measurements. A transistor array was soldered to the stepper motor to allow for precise control of the motor spindle. An Arduino Uno microcontroller was connected to the transistor array and LEDs and programmed to automate spectral intensity measurement of the capillary tubes following a fixed time interval.

We utilized steel capillary tubes of size 50 mm × 1.59mm. × 0.762 mm. (L × O.D. × I.D.) to hold the samples. Alternatively, glass capillary tubes (Drummond Scientific) of similar size can also be used. However, in this case the ends of the tubes must be coated with paint to prevent excess light from the LEDs leaking into the fiber-optic detector. During sample loading, 4µl liquid culture droplets were individually pipetted onto a clean substrate and then loaded into the tubes via capillary action. The capillary tubes were sterilized prior to loading through autoclaving. Following loading, tubes were inserted into the sample holder in a configuration that allows light from the LEDs to pass through the sample and into the fiber-optic detector. Since the volume capacity of the capillary tubes was higher than the sample volume of 4µl, the tubes were loaded with the fluid-filled side near the light-source as this configuration was determined to yield higher signal-to-noise ratios. During susceptibility testing, the cAST platform was placed inside a benchtop incubator (Corning) set to 37°C. A small portable humidifier was also placed inside the incubator to minimize sample drying during incubation. Every 30 minutes, spectral intensity measurements were automatically taken for each sample and the data were transferred and stored on a computer for processing using OceanView.

4.3.3 Susceptibility testing using cAST platform

The cAST platform was used to test five different organisms: *Escherichia coli* ATCC 25922, *Enterobacter cloacae* ATCC 13047, *Acinetobacter baumannii* ATCC BAA-747, *Pseudomonas aeruginosa* ATCC 27853, and *Escherichia coli* K12 ER2267 (kanamycin resistant). To prepare inoculums for AST, bacteria strains were first streaked on Mueller-Hinton II agar plates (Becton Dickinson) and incubated overnight at 37°C. For the kanamycin resistant *E. coli* K12 strain, the agar was supplemented with kanamycin (MilliporeSigma) at 50μg/ml. Liquid cultures were then prepared by inoculating single colonies from the streak plates into cation-adjusted Mueller-Hinton broth (CAMHB, Becton Dickinson), followed by another overnight incubation at 37°C. To achieve the recommended starting inoculum concentration of 5×10^5 colony-forming units per milliliter (CFU/ml) for AST [81], the overnight culture was first diluted using CAMHB to a 0.5 McFarland standard, which represents a concentration of approximately 1×10^8 CFU/ml. Using a spectrophotometer (VWR V-1200), the OD625nm absorbance corresponding to a 0.5 McFarland standard was verified to be in the range of 0.08 – 0.13 [81]. The diluted culture was next additionally diluted 1:100 in CAMHB media, split into subcultures, and supplemented with varying concentrations of antibiotics and a resazurin (PrestoBlue, Thermo Fisher) solution (10% v/v final) to reach an approximate starting inoculum concentration of 5×10^5 CFU/ml. Resazurin is a redox indicator that is reduced by metabolically active cells into resorufin, leading to significant colorimetric and fluorescent changes in the culture media which can be measured to gauge bacterial growth [80]. The aminoglycoside gentamicin was selected to be the target antibiotic for susceptibility testing since it is classified by the Clinical & Laboratory Standards Institute (CLSI) as a Group A (appropriate for inclusion in primary AST panel) antimicrobial agent for all five of the organisms used in this study

[82]. The *E. coli* K12 strain was additionally tested with kanamycin to characterize its increased resistance to the antibiotic. Antibiotic concentrations used for testing were selected based on the susceptible, intermediate, and resistant breakpoints published by CLSI [82]. For testing, 4µl culture samples were loaded into capillaries and subsequently into the cAST platform for automated spectral intensity measurements every 30 min. over a period of 6 – 8 hours. Positive control samples consisted of bacteria inoculums in CAMHB without the addition of antibiotics and negative control samples consisted of bacteria inoculums in CAMHB with the addition of high concentrations of antibiotics (>3× CLSI resistant breakpoint concentration). Negative control samples were formulated in this manner to account for any interactions between non-viable/non-proliferating bacteria and resazurin.

4.3.4 Data analysis

Spectral data captured by the cAST platform were imported into MATLAB for analysis. Lowess regression smoothing was first applied to smooth spectral data followed by algorithmic identification of peaks in the spectral data. Resazurin's peak absorbance is around 600nm and this peak absorbance exhibits blueshift upon conversion of the dye into resorufin by metabolically active bacteria. A similar blueshift can be observed in the spectral intensity profile upon dye reduction. The difference in peak intensity (peak shift) between a test sample and negative control sample was used as a quantitative indicator of bacterial growth. Time to growth detection was determined using a peak shift threshold as non-susceptible and positive control samples exhibited peak shifts >30nm upon reduction of resazurin.

4.3.5 Susceptibility verification using broth dilution

To verify concentration-dependent susceptibility determined using the cAST platform, broth macrodilution was concurrently conducted as a secondary method to assess

susceptibility. Using the same inoculum preparation steps outlined above, 2ml liquid cultures with approximate starting inoculum concentration of 5×10^5 CFU/ml were supplemented with the same antibiotic concentrations as the capillary samples (without resazurin) and subsequently incubated overnight in a shaking incubator at 37°C. Following incubation, susceptibility was visually determined based on whether turbidity was observed.

4.4 Results

4.4.1 cAST platform

cAST consists of a combination of off-the-shelf components and 3D printed parts, as seen in Figure 11. Key components include a stepper motor, fiber-optic cable, portable spectrometer, light source, and 3D-printed parts designed to hold components in alignment for optical measurements. The underlying principle of operation of cAST is simple – light incident on one end of the capillary tube passes through the sample and is then captured by the fiber-optic cable, with the opaque capillary tube serving as an optical waveguide. The fiber-optic cable is coupled to a portable spectrometer that measures the spectral intensity profile of the captured light, which can be monitored for relative changes that are indicative of bacterial growth and antibiotic susceptibility. With the help of an onboard microcontroller, measurements are automated for multiple samples at an adjustable time interval.

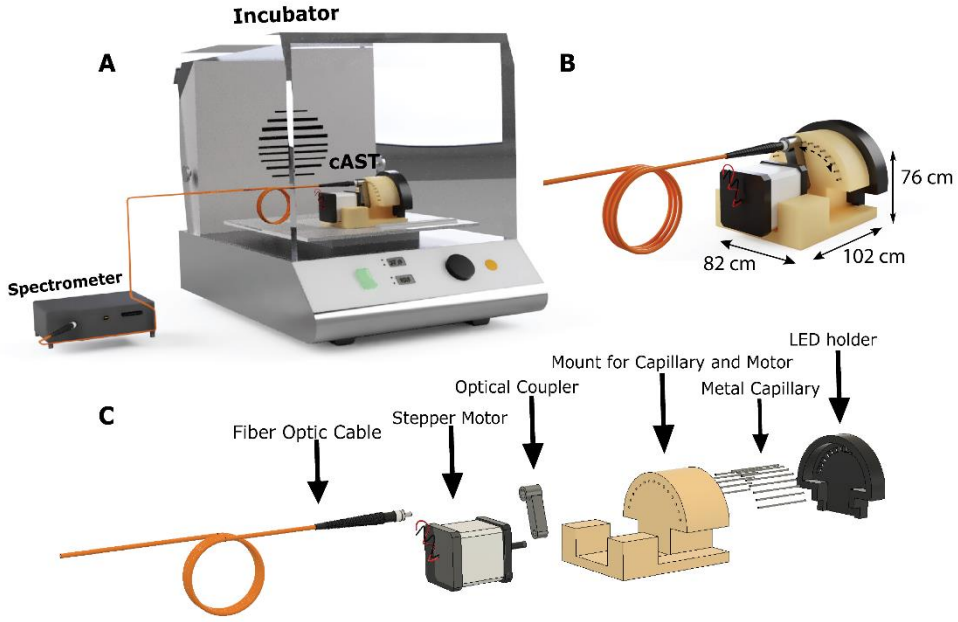

Figure 11. Overview of cAST platform. (**A**) Realistic render of cAST experimental setup. During susceptibility testing, capillary tubes containing bacteria samples are loaded into the cAST device, which is then placed inside a benchtop incubator. A fiber-optic cable connects the cAST device to an external spectrometer, which together with a microcontroller enables automated spectral intensity measurements. (**B**) Dimensions of the cAST device. (**C**) Exploded view of the integral components of the system. The sample holder was designed to allow light from the LEDs to pass through the capillary tube sample and into the fiber-optic detector. During data acquisition, the positioning of the fiber-optic cable is controlled by the stepper motor via rotation of the optical coupler.

The advantages of the cAST platform are three-fold: 1) the system enables accelerated detection of antimicrobial resistance, 2) the system is automated which simplifies workflow when working with multiple samples, and 3) the system facilitates non-contact optical interrogation of small sample volumes (<5 µL, and 3) the system enables non-contact optical interrogation of small sample volumes (< 5µl). The cylindrical form factor of a capillary tube maximizes the optical path length which facilitates optical measurements without requiring optical cavities [83] or traditional microscopy

instruments for readout [76,84], components that are typically required in microfluidic systems which ultimately increase fabrication and operational complexity. In addition to these advantages, the entire cAST system has a small footprint and is built using inexpensive parts making it suitable for use in resource-limited settings.

4.4.2 Bacterial growth in capillary tubes

Prior to susceptibility testing with the cAST platform, we compared detection of bacterial growth in capillary tube versus microwell using three different colorimetric indicators: phenol red, bromomethyl blue, and resazurin. By testing three colorimetric indicators, we wanted to first examine how incubation inside the capillary tube form factor affects bacterial growth and subsequently determine which indicator yields the fastest detection of growth. For all three colorimetric indicators, metabolically active bacteria induce color change in the media over time, which can be quantified through spectral measurements. Phenol red and bromomethyl blue are colorimetric pH indicators that change color in response to the accumulation of bacterial metabolic byproducts such as organic acids. Resazurin is a redox indicator that changes color upon reduction into resorufin by metabolically active cells [80]. Using the test organism *E. coli* diluted to approximately 5×10^5 CFU/ml starting concentration, we loaded 15µl volumes of dye-supplemented cultures into capillary tubes and a 384-microwell plate and incubated the samples at 37°C. Sample color change over time was quantified by measuring sample absorbance in the 350nm – 650nm range using a microplate reader. Capillary samples were dispensed into a microplate at time of measurement to enable use of the plate reader. The difference in peak absorbance (peak shift) between a test sample and negative control sample (no bacteria) was used as a quantitative indicator of bacterial growth. As shown in Fig. 12A, incubation inside the capillary form factor accelerated growth detection relative to incubation inside microwell and amongst the

three colorimetric indicators tested, resazurin yielded the fastest detection of growth. In fact, resazurin in the capillary form factor yielded a time to growth detection that was 45 minutes faster than resazurin in the microwell format.

Using the same spectral measurement approach, we next investigated the impact of capillary tube inner diameter size on bacterial growth and time to growth detection. *E. coli* inoculated media supplemented with resazurin, with 5×10^5 CFU/ml approximate starting concentration, was incubated inside capillary tubes with three different inner diameters (0.45mm, 0.70mm., and 0.76 mm.) and incubated at 37°C. Sample color change over time, corresponding to bacterial growth, was quantified by measuring sample absorbance in the 350nm – 650nm range. Because of the drastic wavelength shift of resazurin reduction observed in the previous experiment (Fig. 12A), time to growth detection was determined as the timepoint at which a wavelength shift of greater than 25nm was detected. As shown in Fig. 12B, an inversely proportional relationship was observed between capillary tube inner diameter and time to growth detection.

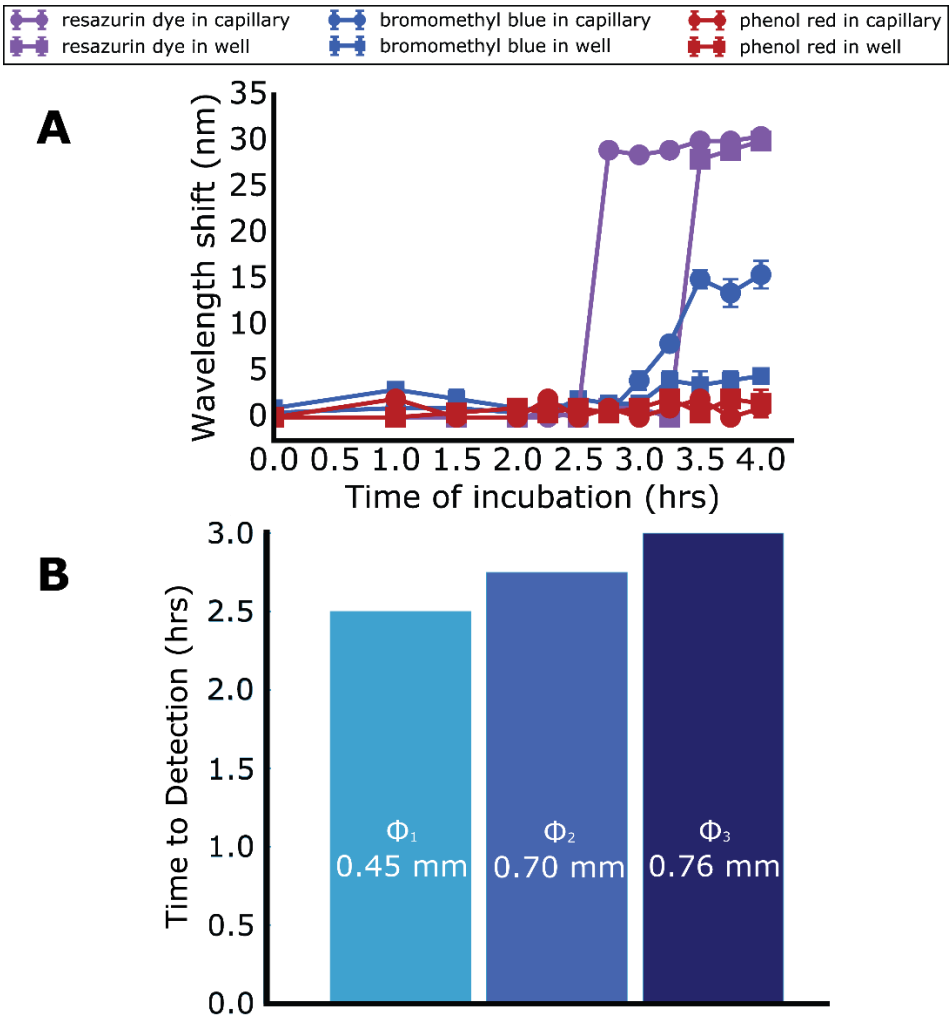

Figure 12. Comparison of *E. coli* growth in capillary tube and microwell. (**A**) Comparison of detection of bacterial growth in capillary tubes and microwell using three different colorimetric indicators: phenol red, bromomethyl blue, and resazurin. Bacterial metabolism induced color change in the media was tracked over time by measuring sample absorbance in the 350nm – 650nm range. The difference in peak absorbance (peak wavelength shift) between a test sample and negative control sample (dye-supplemented media without bacteria) was used as a quantitative indicator of bacterial growth. Incubation inside capillary tubes with the dye resazurin was observed to yield the fastest time to growth detection. Error-bars denote one standard deviation (n=3). (**B**) Impact of capillary tube inner diameter on time to growth detection. Inoculated media supplemented with resazurin was incubated inside capillary tubes with different inner diameters, represented by Φ_1,Φ_2 and Φ_3. Bacterial growth was tracked over time by measuring absorbance and determining peak wavelength shift relative to a negative control sample. Time to detection was determined as the timepoint at which a wavelength shift of greater than 25nm was detected. An inversely proportional relationship was observed between capillary tube inner diameter and time to growth detection.

4.4.3 cAST enabled susceptibility testing

The cAST platform was designed to capitalize on the phenomenon of faster observed growth of bacteria in capillary format in the context of susceptibility testing. We hypothesize that faster growth, evidenced by faster reduction of resazurin, is due to optimal bacteria and nutrient distribution in the capillary format. As shown in the comparison in Fig. 13C & D, we hypothesize that the small length scale of the capillary tube leads to a uniform distribution and diffusion of bacteria within the sample matrix which likely maximizes access to nutrients and optimizes growth. Similar accelerated growth has been observed for bacterial incubation inside microfluidic microchannels with large surface area-to-volume ratios [78].

As shown in Fig. 13A, cAST enabled susceptibility testing is based on the principle that bacterial inhibition by antibiotics will limit the reduction of resazurin into resorufin. On the other hand, non-susceptible/resistant bacteria will proliferate and reduce resazurin into resorufin, thereby inducing significant changes in the color of the sample media over time. Instead of a spectrophotometer, a portable spectrometer was used to monitor color change due to its smaller footprint and the ability to make measurements in-incubator in real-time without interrupting sample incubation. The spectral intensity profile change corresponding to the reduction of resazurin is shown in Fig. 13B.

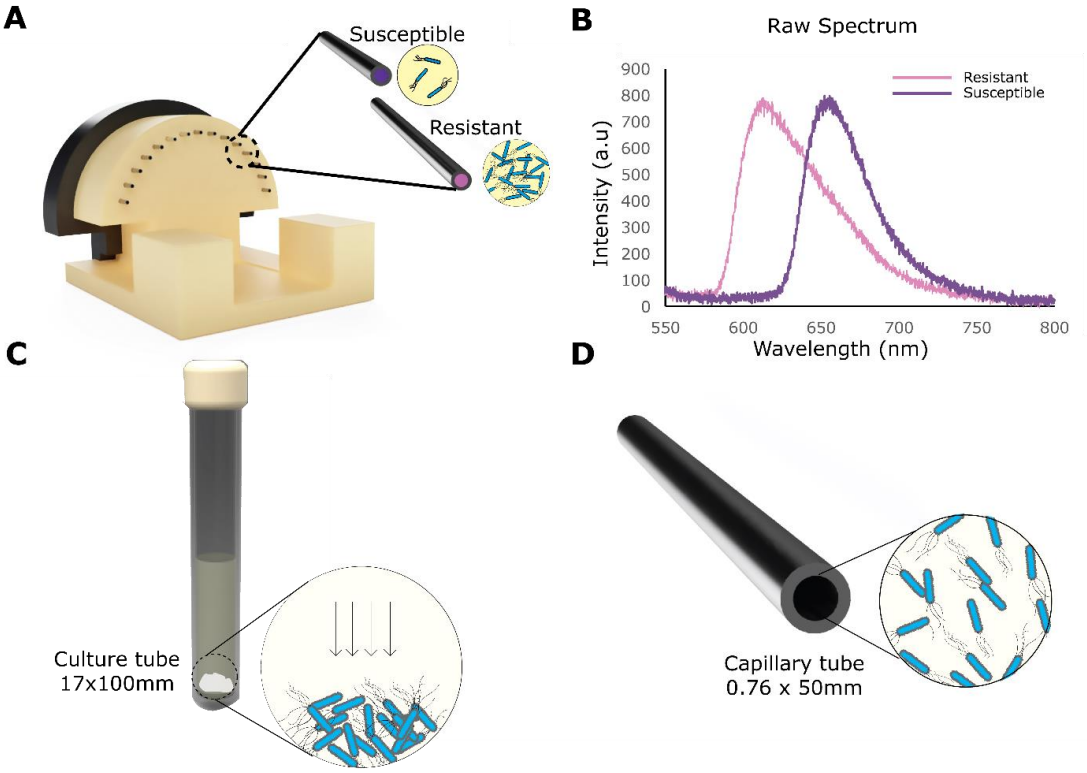

Figure 13. Antibiotic susceptibility testing in capillary format. (**A**) Schematic of cAST setup illustrating use of resazurin as colorimetric indicator for phenotypic detection of bacterial growth. For bacteria uninhibited by a particular antibiotic concentration, subsequent proliferation over time leads to the reduction of resazurin into resorufin, which is characterized by a significant change in the color of the sample media. (**B**) Sample color change over time can be quantified through spectral measurements – either through measuring sample absorbance (using benchtop spectrophotometer) or through measuring the spectral intensity profile of light (using portable spectrometer as part of cAST platform) that pass through the sample. Changes in the peak absorbance/intensity wavelength of the sample relative to a negative control provide a quantitative indicator of bacterial growth. (**C**) and (**D**) Hypothesized advantage of sample incubation inside capillary tubes compared to other form factors. In a large culture tube, the bacteria settle at the bottom as they grow and create an uneven growth environment. The relatively small inner diameter of the capillary, however, leads to a uniform distribution of bacteria within the sample matrix which maximizes access to nutrients and optimizes growth.

4.4.4 Susceptibility testing of clinically relevant organisms

The cAST platform was used to test five different organisms: *Escherichia coli* ATCC 25922, *Enterobacter cloacae* ATCC 13047, *Acinetobacter baumannii* ATCC BAA-747, *Pseudomonas aeruginosa* ATCC 27853, and *Escherichia coli* K12 ER2267 (kanamycin resistant). These opportunistic pathogens are among the prominent causes

of hospital-acquired infections and are frequently drug resistant [85]. We tested each organism's susceptibility to the aminoglycoside gentamicin as this antibiotic is classified by the Clinical & Laboratory Standards Institute (CLSI) as a Group A (appropriate for inclusion in primary AST panel) antimicrobial agent against all five of the selected organisms [82]. The antibiotic concentrations we tested (1, 2, 4, and 50μg/ml) were selected taking into consideration the susceptible, intermediate, and resistant breakpoint concentrations published by CLSI. The *E. coli* K12 strain was additionally tested with kanamycin (50, and 100μg/ml) to characterize its increased resistance to the antibiotic (Fig. 14A). For each organism, we collected 6-8 hours of data using the cAST platform and the susceptibility results are shown in Fig. 4C. Due to resazurin's high spectral change upon reduction, the time point at which growth was detected can be determined through thresholding either spectral wavelength shift data or the associated slope data (Fig. 14B). As expected for a phenotypic susceptibility testing technique, a strong positive correlation was observed between time to growth detection and organism doubling time (Fig. 14D). Susceptibility results are summarized in Fig. 14E and individual data for each organism is noted in Appendix B. cAST-enabled susceptibility results were verified against broth macrodilution, which showed unanimous agreement but required significantly longer incubation times.

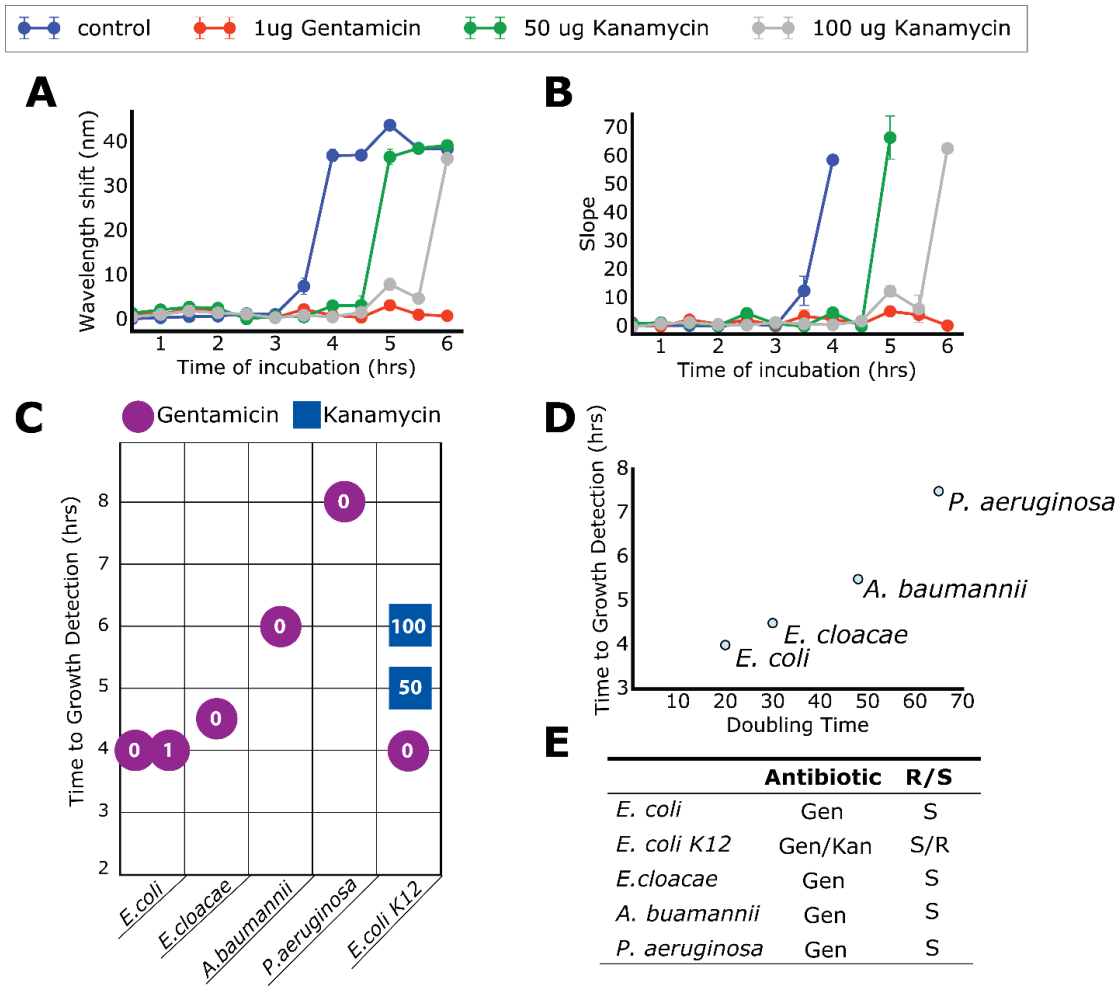

E

	Antibiotic	R/S
E. coli	Gen	S
E. coli K12	Gen/Kan	S/R
E.cloacae	Gen	S
A. buamannii	Gen	S
P. aeruginosa	Gen	S

Figure 14. Multi-organism susceptibility testing data from cAST platform. (**A**) Peak intensity wavelength shift over time for a kanamycin resistant *E. coli* strain. The difference in spectral peak intensity (wavelength shift) between a test sample and negative control sample provides a quantitative indicator of bacterial growth. The *E. coli* strain was tested with gentamicin (CLSI Group A antimicrobial agent) as well as kanamycin to characterize its increased resistance. For a non-inhibiting antibiotic concentration, bacterial proliferation induced reduction of resazurin led to significant changes in the sample spectral intensity profile, as evidenced by drastic increases in peak wavelength shift. Error-bars denote one standard deviation. (**B**) Instantaneous slopes of peak intensity wavelength shift data. (**C**) Antibiotic susceptibility data for five organisms*: E. coli*, *E. cloacae*, *A. baumannii*, *P. aeruginosa*, and a kanamycin resistant *E. coli* strain. The markers denote the time at which wavelength shift/slope exceeded a threshold, representing detection of organism growth. The letter C represents the positive control group and the numbers denote antibiotic concentrations in µg/ml. Gentamicin is represented by a square marker and kanamycin is represented by a triangular marker. (**D**) Relationship between time to detection and organism doubling time. (**E**) Summary of AST results. Susceptibility results were verified through broth macrodilution.

4.5 Discussion

It is estimated that for patients with septic shock, every hour that goes by without appropriate antibiotic administration results in a 7.6% drop in survival rate [68]. In time sensitive situations, rapid AST techniques are crucial for expediting the administration of effective antibiotic therapy. In this work, we demonstrated a novel rapid AST technique based on optical interrogation of organisms incubated inside a capillary tube form factor – which was empirically determined to accelerate time to growth detection and readout. In particular, we were first able to demonstrate off-device that incubation in the capillary form factor yielded an approximately 25% faster readout compared to incubation in the microwell format, which is commonly used in microdilution AST methods. Next, we demonstrated development of the cAST platform, a robust device setup that leverages 3D-printed and off-the-shelf components to enable automated optical measurements of samples housed in capillary format. With the use of a resazurin redox indicator, we were able to demonstrate reliable AST results, for five different clinically relevant organisms within 4-8 hours, making it comparable in performance to microfluidic approaches demonstrated in literature (14-17). However, the simplicity of the testing setup, the ease of operation and the small footprint of the device make cAST a superior platform for use in resource-limited and translational settings.

The cAST system offers several advantages relative to other AST methods. Firstly, the low sample volume requirement (<5µl) limits reagent consumption and is conducive to minimizing the number of pre-AST incubation steps needed to scale up organism concentration. For instance, AST can potentially be directly conducted using an inoculum from patient sample or streak plate. Secondly, the platform utilizes commercially available capillary tubes, which are reusable following sterilization and are of lower fabrication and operational complexity compared to small volume sample-

holding consumables used in microfluidic systems [75–78]. Thirdly, the small footprint and portability of the platform makes it amenable for use in point-of-care settings.

The primary innovation of our work revolves around the discovery that bacterial incubation in the capillary form factor appears to enhance the growth rate, as evidenced by faster reduction of resazurin relative to bacterial incubation in microwells. We hypothesize that this phenomenon is due to two possible reasons: 1) capillary forces within the tube induce a uniform distribution of bacteria and nutrients that optimizes growth or 2) bacterial confinement within small diameter capillary tubes facilitates nutrient-seeking chemotaxis behavior that promotes growth [86,87]. It is interesting to note the inverse correlation we observed between tube inner diameter and time to growth detection. Smaller inner diameter tubes further accelerated growth, possibly as a result of greater internal capillary forces. In the context of optical measurements, however, decreasing the tube inner diameter comes at the cost of reducing signal output. For this reason, the bulk of our experiments were conducted using tubes with 0.76 mm inner diameter, which provided an optimal balance between accelerated growth and optical signal intensity.

To further improve user-friendliness of the cAST platform, antibiotics and resazurin can be lyophilized directly inside capillary tubes – thereby simplifying the workflow and reducing the number of manual pipetting/dilution steps needed. Through this approach, tubes can be pre-loaded with different antibiotics at varying concentrations and all that is needed to initiate testing would be rehydration of the lyophilized components with inoculated culture media. A detachable sample holder with a circular mesh pattern can additionally be developed to increase the number of samples that can be tested in parallel, thereby increasing multiplexing potential. As the spectrometer is the most expensive component of the current system, we envision a less expensive system can be achieved by replacing the spectrometer with a photodiode and optical filter set at the

appropriate wavelength to detect reduction of resazurin. The addition of internal heating capabilities to the system will enable incubator-free AST, further improving portability and decreasing the infrastructure required for susceptibility testing. The reduction of resazurin into resorufin induces both fluorescent and colorimetric changes in the culture media. The addition of fluorescence detection to the cAST platform can increase the sensitivity of growth detection but comes with the tradeoffs of increased cost and complexity.

In summary, we developed a capillary-based platform for rapid phenotypic antimicrobial susceptibility testing. Our platform was designed to take advantage of the phenomenon that bacterial incubation inside capillary tubes enhanced growth, which in turn can be leveraged for faster susceptibility testing. We demonstrated that our system was able to detect bacterial growth and determine antibiotic susceptibility for several clinically relevant organisms within 4-8 hours of incubation. The cAST platform is an accessible alternative to conventional rapid AST methods and its simplicity makes it well-suited for use in resource-limited settings.

CHAPTER FIVE

CONCLUSIONS AND FUTURE DIRECTIONS

5.1 Engineering Biomedical Technologies for the developing world

Point-of-care testing presents a suitable theme for the development of diagnostic tests of the present and future. In chapters 2 through 4 of this dissertation, I detail the development of new and unique biomedical technologies that are aimed at translating conventional laboratory testing from the benchtop to the bedside. While each of the technologies is centered around a tackling a different biomedical challenge, the underlying theme is the same: engineering technologies that are appropriate for use at the point-of-care and by extension, in resource-limited settings.

In chapter 2, I highlight a novel method for assessing Vitamin D deficiency in human finger-stick blood with the help of a rapid diagnostic test. Vitamin D is notoriously difficult to detect even with conventional laboratory equipment as the protocols for testing involve laborious and time-consuming processing steps. With the help of the Nutriphone platform, we were able to demonstrate a quick and easy alternative to perform quantitative Vitamin D detection, with the help of a unique elution buffer that denatures the binding proteins in situ. This allows for a quantitative test to be conducted within 30 minutes with only a few drops of blood. This method could serve as a platform to perform large-scale nutritional screening in developing countries and is a promising step towards the development of personalized medical devices for the purpose of nutritional deficiency assessment.

In chapter 3, I discuss H.E.R.M.E.S, a unique sample processing technology that can help bridge the gap in demand and access to decentralized blood testing. H.E.R.M.E.S uses a novel magnetic bead-based approach to achieve the separation of blood from plasma in small volumes of sample. The separation is highly efficient and can be achieved in under 2 minutes at less than $2 per test by using a simple and portable benchtop device. This device is easy to use and requires minimal user intervention. H.E.R.M.E.S was designed to help improve the performance of existing rapid diagnostic tests, like the Vitamin D rapid diagnostic test mentioned in chapter 2. However, the scope of application extends beyond POC tests and is virtually compatible with any blood-based diagnostic test. Therefore, we strongly believe H.E.R.M.E.S can help usher in a new generation of blood-based diagnostic tests that were previously difficult to incorporate at the point of the care because of the requirement of centrifugation. H.E.R.M.E.S also has the potential to revolutionize molecular testing at the point of care and help bring highly accurate assays like PCR to the bedside.

In chapter 4, I detail our initial efforts in the development of a platform for the accelerated assessment of antimicrobial resistance of bacterial organisms. cAST uses a unique capillary form factor, a resazurin dye and a portable spectrophotometer to give high resolution, real time viability information on bacterial organisms. We demonstrated that the simple act of incubating a bacterial organism in a capillary form factor speeds up the growth process by approximately 25% in comparison to a traditional well plate. We also prove the validity of cAST with the help of five clinical organisms and were able to demonstrate that cAST can provide accurate AST results within 4-8 hours of bacterial growth. cAST offers similar diagnostic performance to that

of other works in literature in a simple, easy to use setup that does not require specialized equipment. Further, the setup, composed entirely of off-the-shelf-parts and 3D printed units, is extremely suitable for use at the point of care and in resource limited settings. The underlying technology of cAST makes it useful for currently existing diagnostic tools as the primary innovation is universally applicable to most optical detection methods. Future work on this project will include the possibility of designing a refined version of cAST that uses simple electrical components like a photodiode to make the necessary measurements. For resource-limited settings, cAST can be implemented as a qualitative assay with the help of clear glass capillaries. In this use-case, the resistance can be directly inferred by visual inspection of a color change, thereby further eliminating the need for any specialized equipment.

APPENDIX A: SUPPLEMENTAL DATA FOR H.E.R.M.E.S

Table A1: Demographic Information of samples used for human trial. Abbreviations: Caucasian (Cauc), African American (Af Am), Hispanic (Hisp).

Sample #	Ethnicity	Age	Gender	Hematocrit %	Blood type
1	Cauc	49	M	56	O+
2	Af Am	54	M	55	A+
3	Cauc	48	M	45	O-
4	Hisp	33	M	53	A+
5	Cauc	46	M	47	A-
6	Cauc	41	M	48	A-
7	Af Am	20	M	53	A+
8	Af Am	51	M	47	B+
9	Hisp	51	M	47	O-
10	Hisp	45	M	48	A+
11	Cauc	55	F	52	O-
12	Af Am	31	F	46	O-
13	Cauc	39	F	57	O-
14	Cauc	36	F	53	O-
15	Hisp	58	F	42	B-

Table A2: Cost breakdown of raw materials for each test.

Raw material	**Cost per test ($)**
Magnetic beads	0.55
Aggregation Agent	1.3
Conjugation Reagents	0.135
Total Cost	**1.985**

APPENDIX B: SUPPLEMENTAL DATA FOR cAST

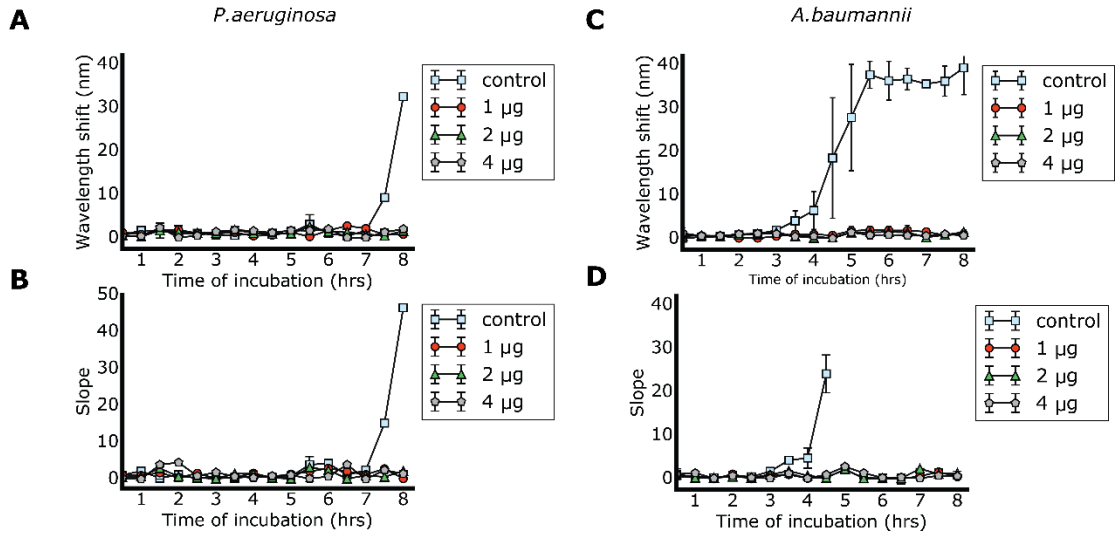

Figure B1: Real-time wavelength shift and slope data for A) and B) P.aeruginosa and C) and D) A.baumannii

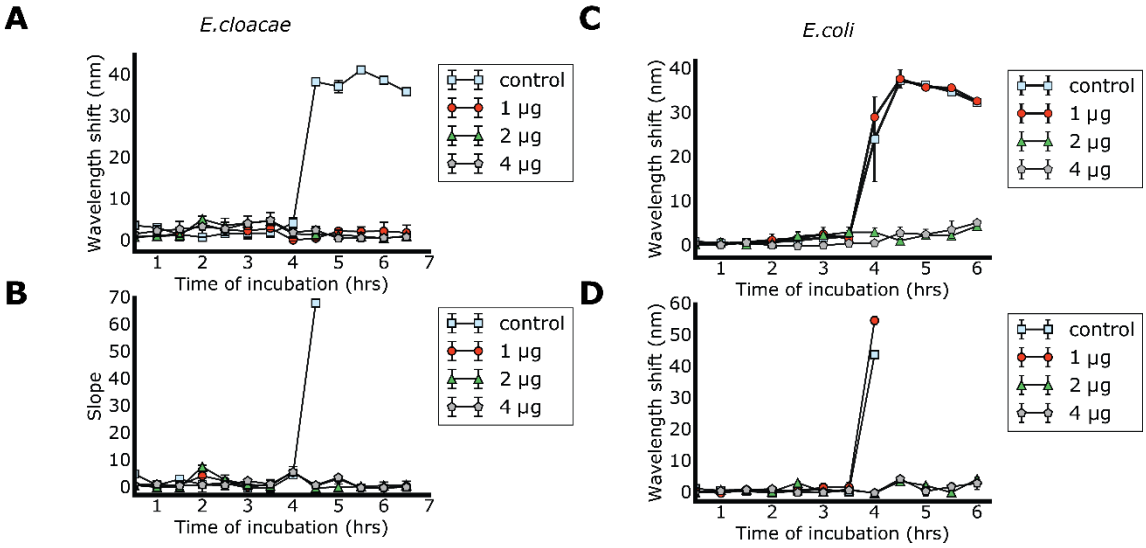

Figure B2: Real-time wavelength shift and slope data for A) and B) E.cloacae and C) and D) E.coli

REFERENCES

1. Ross, A. C., Taylor, C. L., Yaktine, A. L. & Valle, H. B. D. *Dietary Reference Intakes for Calcium and Vitamin D*. (National Academies Press (US), 2011).

2. Norman, A. W. From vitamin D to hormone D: fundamentals of the vitamin D endocrine system essential for good health. *Am. J. Clin. Nutr.* **88**, 491S-499S (2008).

3. Calvo, M. S., Whiting, S. J. & Barton, C. N. Vitamin D Intake: A Global Perspective of Current Status. *J. Nutr.* **135**, 310–316 (2005).

4. Wagner, C. L. & Greer, F. R. Prevention of Rickets and Vitamin D Deficiency in Infants, Children, and Adolescents. *Pediatrics* **122**, 1142–1152 (2008).

5. Holick, M. F. Vitamin D: importance in the prevention of cancers, type 1 diabetes, heart disease, and osteoporosis. *Am. J. Clin. Nutr.* **79**, 362–371 (2004).

6. Fabri, M. *et al.* Vitamin D Is Required for IFN-γ–Mediated Antimicrobial Activity of Human Macrophages. *Sci. Transl. Med.* **3**, 104ra102-104ra102 (2011).

7. Houghton, L. A. & Vieth, R. The case against ergocalciferol (vitamin D2) as a vitamin supplement. *Am. J. Clin. Nutr.* **84**, 694–697 (2006).

8. Tripkovic, L. *et al.* Comparison of vitamin D2 and vitamin D3 supplementation in raising serum 25-hydroxyvitamin D status: a systematic review and meta-analysis. *Am. J. Clin. Nutr.* **95**, 1357–1364 (2012).

9. Holick, M. F. *et al.* Evaluation, Treatment, and Prevention of Vitamin D Deficiency: an Endocrine Society Clinical Practice Guideline. *J. Clin. Endocrinol. Metab.* **96**, 1911–1930 (2011).

10. Forrest, K. Y. Z. & Stuhldreher, W. L. Prevalence and correlates of vitamin D deficiency in US adults. *Nutr. Res. N. Y. N* **31**, 48–54 (2011).

11. Wootton, A. M. Improving the Measurement of 25-hydroxyvitamin D. *Clin. Biochem. Rev.* **26**, 33 (2005).

12. Carter, G. D. Accuracy of 25-Hydroxyvitamin D Assays: Confronting the Issues. *http://www.eurekaselect.com* Available at: http://www.eurekaselect.com/72893/article. (Accessed: 19th April 2017)

13. Edelstein, S. Vitamin D Binding Proteins. *Vitam. Horm.* **32**, 407–428 (1975).

14. Bikle, D. D. *et al.* Assessment of the Free Fraction of 25-Hydroxyvitamin D in Serum and Its Regulation by Albumin and the Vitamin D-Binding Protein. *J. Clin. Endocrinol. Metab.* **63**, 954–959 (1986).

15. Bouillon, R., Assche, F. A. V., Baelen, H. V., Heyns, W. & Moor, P. D. Influence of the Vitamin D-binding Protein on the Serum Concentration of 1,25-Dihydroxyvitamin D3: SIGNIFICANCE OF THE FREE 1,25-DIHYDROXYVITAMIN D3 CONCENTRATION. *J. Clin. Invest.* **67**, 589 (1981).

16. Pee, S. de & Dary, O. Biochemical Indicators of Vitamin A Deficiency: Serum Retinol and Serum Retinol Binding Protein. *J. Nutr.* **132**, 2895S-2901S (2002).

17. Hix, J. *et al.* Validation of a rapid enzyme immunoassay for the quantitation of retinol-binding protein to assess vitamin A status within populations. *Eur. J. Clin. Nutr.* **60**, 1299–1303 (2006).

18. Craft, N. E. Innovative Approaches to Vitamin A Assessment. *J. Nutr.* **131**, 1626S-1630S (2001).

19. Gamble, M. V. *et al.* Retinol binding protein as a surrogate measure for serum retinol: studies in vitamin A–deficient children from the Republic of the Marshall Islands. *Am. J. Clin. Nutr.* **73**, 594–601 (2001).

20. Kartalov, E. P. *et al.* Internally calibrated quantification of protein analytes in human serum by fluorescence immunoassays in disposable elastomeric microfluidic devices. *Electrophoresis* **29**, 5010 (2008).

21. Dimov, I. K. *et al.* Stand-alone self-powered integrated microfluidic blood analysis system (SIMBAS). *Lab. Chip* **11**, 845–850 (2011).

22. Lee, S., Oncescu, V., Mancuso, M., Mehta, S. & Erickson, D. A smartphone platform for the quantification of vitamin D levels. *Lab. Chip* **14**, 1437–1442 (2014).

23. Laboratory Procedure Manual for Diasorin(formerly Incstar) 25-OH-D assay.

24. Tan, S. C. & Yiap, B. C. DNA, RNA, and Protein Extraction: The Past and The Present. *J. Biomed. Biotechnol.* **2009**, (2009).

25. Arakawa, T., Kita, Y. & Timasheff, S. N. Protein precipitation and denaturation by dimethyl sulfoxide. *Biophys. Chem.* **131**, 62–70 (2007).

26. Tanford, C. Protein Denaturation. *Adv. Protein Chem.* **23**, 121–282 (1968).

27. DeLong, E. R., DeLong, D. M. & Clarke-Pearson, D. L. Comparing the areas under two or more correlated receiver operating characteristic curves: a nonparametric approach. *Biometrics* **44**, 837–845 (1988).

28. Intakes, I. of M. (US) S. C. on the S. E. of D. R. *Dietary Reference Intakes for Calcium, Phosphorus, Magnesium, Vitamin D, and Fluoride*. (National Academies Press (US), 1997).

29. Global Blood Testing Market Size & Share | Industry Report, 2018-2024. Available at: https://www.grandviewresearch.com/industry-analysis/blood-testing-market. (Accessed: 14th June 2018)

30. Al-Soud, W. A. & Radstrom, P. Purification and Characterization of PCR-Inhibitory Components in Blood Cells. *J. Clin. Microbiol.* **39**, 485–493 (2001).

31. Mabey, D., Peeling, R. W., Ustianowski, A. & Perkins, M. D. Diagnostics for the developing world: Tropical infectious diseases. *Nat. Rev. Microbiol.* **2**, 231–240 (2004).

32. Recommendations for Clinical Laboratory Improvement Amendments of 1988 (CLIA) WaiverApplications for Manufacturers of In Vitro Diagnostic Device - Guidance for Industry and Food and Drug Adminstration Staff. (2008).

33. Liu, C. *et al.* Membrane-Based, Sedimentation-Assisted Plasma Separator for Point-of-Care Applications. *Anal. Chem.* **85**, 10463–10470 (2013).

34. Posthuma-Trumpie, G. A., Korf, J. & van Amerongen, A. Lateral flow (immuno)assay: its strengths, weaknesses, opportunities and threats. A literature survey. *Anal. Bioanal. Chem.* **393**, 569–582 (2009).

35. Xu, Q. *et al.* Development of lateral flow immunoassay system based on superparamagnetic nanobeads as labels for rapid quantitative detection of cardiac troponin I. *Mater. Sci. Eng. C* **29**, 702–707 (2009).

36. Son, J. H. *et al.* Hemolysis-free blood plasma separation. *Lab Chip* **14**, 2287–2292 (2014).

37. Mielczarek, W. S., Obaje, E. A., Bachmann, T. T. & Kersaudy-Kerhoas, M. Microfluidic blood plasma separation for medical diagnostics: is it worth it? *Lab. Chip* **16**, 3441–3448 (2016).

38. Kersaudy-Kerhoas, M. & Sollier, E. Micro-scale blood plasma separation: from acoustophoresis to egg-beaters. *Lab. Chip* **13**, 3323 (2013).

39. Gossett, D. R. *et al.* Label-free cell separation and sorting in microfluidic systems. *Anal. Bioanal. Chem.* **397**, 3249–3267 (2010).

40. Bhagat, A. A. S. *et al.* Microfluidics for cell separation. *Med. Biol. Eng. Comput.* **48**, 999–1014 (2010).

41. Chen, X., Cui, D., Liu, C. & Li, H. Microfluidic chip for blood cell separation and collection based on crossflow filtration. *Sens. Actuators B Chem.* **130**, 216–221 (2008).

42. Chin, C. D., Linder, V. & Sia, S. K. Commercialization of microfluidic point-of-care diagnostic devices. *Lab. Chip* **12**, 2118 (2012).

43. Brown, J. *et al.* A Hand-Powered, Portable, Low-Cost Centrifuge for Diagnosing Anemia in Low-Resource Settings. *Am. J. Trop. Med. Hyg.* **85**, 327–332 (2011).

44. Wong, A. P., Gupta, M., Shevkoplyas, S. S. & Whitesides, G. M. Egg beater as centrifuge: isolating human blood plasma from whole blood in resource-poor settings. *Lab. Chip* **8**, 2032 (2008).

45. Bhamla, M. S. *et al.* Hand-powered ultralow-cost paper centrifuge. *Nat. Biomed. Eng.* **1**, 0009 (2017).

46. Mariella, R. Sample preparation: the weak link in microfluidics-based biodetection. *Biomed. Microdevices* **10**, 777–784 (2008).

47. Street, P. Requirements for high impact diagnostics in the developing world. 8

48. Dineva, M. A., Mahilum-Tapay, L. & Lee, H. Sample preparation: a challenge in the development of point-of-care nucleic acid-based assays for resource-limited settings. *The Analyst* **132**, 1193 (2007).

49. Plebani, M. Does POCT reduce the risk of error in laboratory testing? *Clin. Chim. Acta* **404**, 59–64 (2009).

50. Caldarelli-Stefano, R., Vago, L., Bonetto, S., Nebuloni, M. & Costanzi, G. Use of magnetic beads for tissue DNA extraction and IS6110 Mycobacterium tuberculosis PCR. *Mol. Pathol.* **52**, 158–160 (1999).

51. Fiedler, G. M. *et al.* Standardized Peptidome Profiling of Human Urine by Magnetic Bead Separation and Matrix-Assisted Laser Desorption/Ionization Time-of-Flight Mass Spectrometry. *Clin. Chem.* **53**, 421–428 (2007).

52. Sista, R. S. *et al.* Heterogeneous immunoassays using magnetic beads on a digital microfluidic platform. *Lab. Chip* **8**, 2188 (2008).

53. Tang, D., Zhong, Z., Niessner, R. & Knopp, D. Multifunctional magnetic bead-based electrochemical immunoassay for the detection of aflatoxin B1 in food. *The Analyst* **134**, 1554 (2009).

54. Tripathi, S., Prabhakar, A., Kumar, N., Singh, S. G. & Agrawal, A. Blood plasma separation in elevated dimension T-shaped microchannel. *Biomed. Microdevices* **15**, 415–425 (2013).

55. Yang, X., Forouzan, O., Brown, T. P. & Shevkoplyas, S. S. Integrated separation of blood plasma from whole blood for microfluidic paper-based analytical devices. *Lab Chip* **12**, 274–280 (2012).

56. Srinivasan, B. *et al.* iron Phone: Mobile device-coupled point-of-care diagnostics for assessment of iron status by quantification of serum ferritin. *Biosens. Bioelectron.* **99**, 115–121 (2018).

57. Yeh, E.-C. *et al.* Self-powered integrated microfluidic point-of-care low-cost enabling (SIMPLE) chip. *Sci. Adv.* **3**, e1501645 (2017).

58. Whitby, D. *et al.* Detection of Kaposi sarcoma associated herpesvirus in peripheral blood of HIV-infected individuals and progression to Kaposi's sarcoma. *The Lancet* **346**, 799–802 (1995).

59. Wang, W.-K. *et al.* Detection of Dengue Virus Replication in Peripheral Blood Mononuclear Cells from Dengue Virus Type 2-Infected Patients by a Reverse Transcription-Real-Time PCR Assay. *J. Clin. Microbiol.* **40**, 4472–4478 (2002).

60. Sigurdson, A. J. *et al.* Kin-cohort estimates for familial breast cancer risk in relation to variants in DNA base excision repair, BRCA1 interacting and growth factor genes. *BMC Cancer* **4**, (2004).

61. Lu, Z. *et al.* Rapid diagnostic testing platform for iron and vitamin A deficiency. *Proc. Natl. Acad. Sci.* **114**, 13513–13518 (2017).

62. Ventola, C. L. The antibiotic resistance crisis: part 1: causes and threats. *P T Peer-Rev. J. Formul. Manag.* **40**, 277–83 (2015).

63. CDC. *Antibiotic resistance threats in the United States, 2013*. *United States Department of Health and Human Services* (2013). doi:CS239559-B

64. Ventola, C. L. The antibiotic resistance crisis: part 2: management strategies and new agents. *P T Peer-Rev. J. Formul. Manag.* **40**, 344–52 (2015).

65. Jorgensen, J. H., Ferraro, M. J., Jorgensen, J. H. & Ferraro, M. J. Antimicrobial Susceptibility Testing: A Review of General Principles and Contemporary Practices. *Clin. Infect. Dis.* **49**, 1749–1755 (2009).

66. Balouiri, M., Sadiki, M. & Ibnsouda, S. K. Methods for in vitro evaluating antimicrobial activity: A review. *J. Pharm. Anal.* **6**, 71–79 (2016).

67. Kuper, K. M., Boles, D. M., Mohr, J. F. & Wanger, A. Antimicrobial Susceptibility Testing: A Primer for Clinicians. *Pharmacotherapy* **29**, 1326–1343 (2009).

68. Ferrer, R. *et al.* Empiric antibiotic treatment reduces mortality in severe sepsis and septic shock from the first hour: results from a guideline-based performance improvement program. *Crit. Care Med.* **42**, 1749–55 (2014).

69. van Belkum, A., Dunne, W. M. & Jr. Next-generation antimicrobial susceptibility testing. *J. Clin. Microbiol.* **51**, 2018–24 (2013).

70. Banerjee, R. *et al.* Randomized Trial of Rapid Multiplex Polymerase Chain Reaction–Based Blood Culture Identification and Susceptibility Testing. *Clin. Infect. Dis.* **61**, 1071–1080 (2015).

71. Choi, J. *et al.* A rapid antimicrobial susceptibility test based on single-cell morphological analysis. *Sci. Transl. Med.* **6**, 267ra174 (2014).

72. Yu, H. *et al.* Phenotypic Antimicrobial Susceptibility Testing with Deep Learning Video Microscopy. *Anal. Chem.* **90**, 6314–6322 (2018).

73. Nordmann, P., Poirel, L. & Dortet, L. Rapid detection of carbapenemase-producing Enterobacteriaceae. *Emerg. Infect. Dis.* **18**, 1503–7 (2012).

74. Pires, J., Novais, A. & Peixe, L. Blue-carba, an easy biochemical test for detection of diverse carbapenemase producers directly from bacterial cultures. *J. Clin. Microbiol.* **51**, 4281–3 (2013).

75. Cira, N. J., Ho, J. Y., Dueck, M. E. & Weibel, D. B. A self-loading microfluidic device for determining the minimum inhibitory concentration of antibiotics. *Lab. Chip* **12**, 1052–9 (2012).

76. Avesar, J. *et al.* Rapid phenotypic antimicrobial susceptibility testing using nanoliter arrays. *Proc. Natl. Acad. Sci. U. S. A.* **114**, E5787–E5795 (2017).

77. Tang, Y., Zhen, L., Liu, J. & Wu, J. Rapid Antibiotic Susceptibility Testing in a Microfluidic pH Sensor. *Anal. Chem.* **85**, 2787–2794 (2013).

78. Chen, C. H. *et al.* Antimicrobial Susceptibility Testing Using High Surface-to-Volume Ratio Microchannels. *Anal. Chem.* **82**, 1012–1019 (2010).

79. Doern, C. D. The Slow March toward Rapid Phenotypic Antimicrobial Susceptibility Testing: Are We There Yet? *J. Clin. Microbiol.* **56**, e01999-17 (2018).

80. Guerin, Mondido, McClenn & Peasley. Application of resazurin for estimating abundance of contaminant-degrading micro-organisms. *Lett. Appl. Microbiol.* **32**, 340–345 (2001).

81. Wiegand, I., Hilpert, K. & Hancock, R. E. W. Agar and broth dilution methods to determine the minimal inhibitory concentration (MIC) of antimicrobial substances. *Nat. Protoc.* **3**, 163–175 (2008).

82. Clinical and Laboratory Standards Institute. *M100 Performance Standards for Antimicrobial Susceptibility Testing*. (2019).

83. Rushworth, C. M. *et al.* Cavity-enhanced optical methods for online microfluidic analysis. *Chem. Phys. Lett.* **554**, 1–14 (2012).

84. Magnusson, E. B., Halldorsson, S., Fleming, R. M. T. & Leosson, K. Real-time optical pH measurement in a standard microfluidic cell culture system. *Biomed. Opt. Express* **4**, 1749 (2013).

85. Peleg, A. Y. & Hooper, D. C. Hospital-Acquired Infections Due to Gram-Negative Bacteria. *N. Engl. J. Med.* **362**, 1804–1813 (2010).

86. Berg, H. C. & Turner, L. Chemotaxis of bacteria in glass capillary arrays. Escherichia coli, motility, microchannel plate, and light scattering. *Biophys. J.* **58**, 919–30 (1990).

87. Ping, L., Wasnik, V. & Emberly, E. Bacterial motion in narrow capillaries. *FEMS Microbiol. Ecol.* **91**, 1–7 (2015).